

## Accepted Manuscript

Structure based drug design of Pim-1 kinase followed by pharmacophore guided synthesis of Quinolone-based inhibitors

Lubna Swellmeen, Rand Shahin, Yusuf Al-Hiari, Amani Alamiri, Alaa Hasan, Omar Shaheen

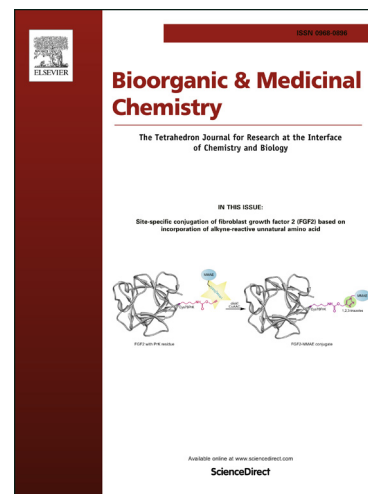
PII: S0968-0896(17)31071-4  
DOI: <http://dx.doi.org/10.1016/j.bmc.2017.07.036>  
Reference: BMC 13873

To appear in: *Bioorganic & Medicinal Chemistry*

Received Date: 17 May 2017  
Revised Date: 18 July 2017  
Accepted Date: 19 July 2017

Please cite this article as: Swellmeen, L., Shahin, R., Al-Hiari, Y., Alamiri, A., Hasan, A., Shaheen, O., Structure based drug design of Pim-1 kinase followed by pharmacophore guided synthesis of Quinolone-based inhibitors, *Bioorganic & Medicinal Chemistry* (2017), doi: <http://dx.doi.org/10.1016/j.bmc.2017.07.036>

This is a PDF file of an unedited manuscript that has been accepted for publication. As a service to our customers we are providing this early version of the manuscript. The manuscript will undergo copyediting, typesetting, and review of the resulting proof before it is published in its final form. Please note that during the production process errors may be discovered which could affect the content, and all legal disclaimers that apply to the journal pertain.



# Structure based drug design of Pim-1 kinase followed by pharmacophore guided synthesis of Quinolone-based inhibitors

*LubnaSwellmeen<sup>a</sup>, Rand Shahin<sup>b</sup>, Yusuf Al-Hiari<sup>c</sup>, Amani Alamiri<sup>b</sup>, Alaa Hasan<sup>a</sup>, Omar Shaheen<sup>d</sup>*

<sup>a</sup>Department of Pharmaceutical Sciences, Faculty of Pharmacy, Zarqa University, Azzarqa, Jordan.

Email: [lswellmeen@zu.edu.jo](mailto:lswellmeen@zu.edu.jo)

<sup>b\*</sup>Corresponding Author,

Department of Pharmaceutical Chemistry, Faculty of Pharmaceutical sciences, Hashemite University, Az-zarqa, Jordan.

Telephone: 00962 799799044.

Email: [r.shahin@hu.edu.jo](mailto:r.shahin@hu.edu.jo)

<sup>c</sup>Department of Pharmaceutical sciences, Faculty of Pharmacy, University of Jordan, Amman, Jordan.

[hiary@ju.edu.jo](mailto:hiary@ju.edu.jo)

<sup>d</sup>Department of Pharmacology, Faculty of Medicine, University of Jordan, Amman, Jordan.

Telephone: 00962 5548511.

Email: [oshaheen@ju.edu.jo](mailto:oshaheen@ju.edu.jo)

**Abstract**

Over expression of Human Phosphatidyl inositol mannoside kinases isoform 1 (Pim-1 kinase) has been reported in several leukemia and solid tumors. Our continuous interest to reveal the secretaries of the mysterious Pim-1 kinase binding pocket has led us to employ a structure based drug design procedure based on receptor-ligand pharmacophore generation protocol implemented in Discovery Studio 4.5 (DS 4.5). Subsequently, we collected 104 crystal structures of Pim-1 kinase from the Protein Data Bank (PDB) and used them to generate pharmacophores based on the anticipated co-crystallized ligand-Pim 1 kinase receptor interactions. All selected pharmacophoric features were enumerated and only those that had corresponding valuable receptor-ligand interactions were retained. This was followed by modeling all pharmacophore combinations and scoring them according to their Receiver Operating Characteristic (ROC) curve analysis parameters as well as a DS.4.5 built-in Genetic Function Algorithm (GFA) validating model. Accordingly, 111 pharmacophores resulted with acceptable ROC performances; **1XWS\_2\_04**, **2BIK\_2\_06**, and **1XWS\_2\_06** (ROC AUC value of: 0.770, 0.743 and 0.741 respectively) were the best pharmacophores. These pharmacophores were employed to guide the synthesis of new series of 7-[(2-Carboxyethyl) amino]-1-substituted-6-fluoro-8-nitro-4-oxo-1,4-dihydro-quinoline-3-carboxylic acid and their reduced 8-amino derivatives. The synthesized compounds were later evaluated for their Pim-1 kinase inhibitory potencies. Of which the most potent illustrated an  $IC_{50}$  value of 0.29  $\mu$ M against Pim-1 kinase.

**Key words:**

Pim 1 kinase, Discovery Studio, Binding pocket, Pharmacophores, Receptor, Quinolone.

**Introduction:**

Human phosphatidyl inositol mannoside kinases (Pim kinases) are a family of serine/threonine kinases composed of three members; Pim-1, Pim-2 and Pim-3. Pim kinases proto oncogenes regulate several signaling pathways which are directly related to the development of numerous malignancies. The Pim-1 kinase isoform (a 313-amino acid kinase) has been specifically reported in the last two decades for its direct role in tumor genesis process in various hematological malignancies, such as lymphoma and acute myeloid leukemia.<sup>1-3</sup> Similarly, over expression of Pim-1 has been linked to several solid tumors such as urothelial and prostate carcinomas.<sup>2-7</sup> Furthermore, developing effective Pim-1 inhibitors is also important to overcome the Pim kinase promoted chemo-resistance of tumor cells through hypoxia-induced chemotherapy resistance.<sup>4,8</sup> Per se, the Pim-1 is considered as a very attractive target for pharmacological inhibition in cancer therapy.

The crystal structure of Pim-1 kinase adopts a two-lobe kinase fold; the N-terminal and the C-terminal. The two lobes are combined with the hinge region amino acids residues, comprising, Glutamine 121, Arginine 122, Proline 123, Glutamine 124 and Valine 126, this hinge region also extends to the Aspartate 128 and Aspartate 131 residues. Along the hinge region resides is the deep Adenosine triphosphate (ATP) binding pocket which encompasses, the phosphate binding loop lying on the top of the ATP binding pocket like a lid (P-loop: residues 46-54), the catalytic loop (C-loop: residues 166-170), and the activation loop (A-loop: residues 191-202).<sup>1-2</sup> Designing new selective kinase inhibitors has been always an issue due to the high degree of conservation in the protein amino acid sequence among different kinases, but the Pim-1 kinase binding pocket is known to have some distinctive features that can be exploited, for example; Pim-1 kinase binding pocket is considered atypical in many aspects; this is due to the presence of the Proline 123 moiety in the hinge region where adenine usually binds via two hydrogen bonds.<sup>7,9</sup> As well, the hydrophobic region I (BR-I) in Pim-1 kinase is distinctively different from other kinases'. So, revealing more possible binding

interactions inside the binding pocket of Pim-1 kinase will open the road towards discovering more selective and specific new inhibitors against this target.

We believe that illuminating the secrets of the mysterious Pim-1 kinase binding pocket and understanding the Pim-1 versus ligand interaction models is of great importance for determining the potential activities of novel Pim-1 kinase inhibitors and designing new ones. In our previously published research project,<sup>7</sup> we designed a QSAR guided ligand-based study for Pim-1 kinase enzyme, and we were able to reveal some of the steric and electronic features that represent the optimal interactions between Pim-1 kinase inhibitors and its binding pocket from the resulted QSAR successful equation. Our interest to reveal even more ambiguous points inside the binding pocket of pim-1 kinase has encouraged us to continue our investigation through another structure based study. Subsequently, our aim of this work is to extract and interpret Pim-1 kinase co-crystallized ligands from the Protein Data Bank (PDB) focusing on X-ray structure complexes, which have a satisfactorily good resolution. A PDB complex does not only contain experimental data but also a reasonable amount of interpretation that can be done by a researcher.<sup>10</sup> In most cases, structure determination efforts focus on the macromolecule (Pim-1 kinase protein, for example), while in our work ligand structures were elucidated then the potential interactions between the ligand and the Pim-1 kinase binding pocket were clarified and explained.

Furthermore, the most successful pharmacophores that resulted from modelling the ligand-receptor interactions were engaged as guiding maps to design new 7-[(2-Carboxyethyl)amino]-1-alkyl-6-fluoro-8-nitro-4-oxo-1,4-dihydro-quinoline-3-carboxylic acid derivatives as novel inhibitors against Pim-1 kinase enzyme. The present study is aiming to explore the key structural requirements for Pim-1 kinase inhibition utilizing combination of the above modeling methods for the design of novel, selective Pim-1 kinase inhibitors.

## 2. Results

Receptor-ligand pharmacophore generation technique models drug-receptor interactions using information derived from co-crystallized ligand contact points with their receptors.<sup>11</sup> HYPOGEN detects a 3D collection of five to six chemical features that reflect the hot contact points between the co-crystallized ligand and the binding pocket in which it was originally entrenched, which delivers a relative configuration for each co-crystallized ligand consistent with their binding modes inside the receptor site. A total of 104 X-ray Pim-1 kinase crystal structure complexes were used in this study. 111 training Hypogens (pharmacophores) were generated, of which only 7 pharmacophores showed acceptable results upon validation with Receiver Operating Characteristic (ROC) analysis as well as a DS.4.5 built-in Genetic Function Algorithm (GFA) validating model. The 7 successful pharmacophores were then engaged as guiding maps to design new quinolone-based series of Pim-1 kinase inhibitors.

### 2.1 Literature survey and data mining

The ChEMBL data base was surveyed to collect as many X-ray crystal structure complexes for Pim-1 kinase as possible. Pim-1 kinase target (**CHEMBL2147**) revealed 104 crystal structures in the Protein Data Bank (<http://www.rcsb.org/>) please refer to SM-1 in supplementary material for the names of all PDB crystal structures used. Altogether, the 104 X-ray crystal structure complexes were collected, cleaned, and then engaged in consequent modelling processes.

### 2.2 Generating receptor-ligand pharmacophores

After employing the receptor-ligand pharmacophore generation procedure, only 111 pharmacophores resulted in a ROC-AUC value above 0.5. **Table 1** shows the PDB code of the Pim-1 kinase crystals that displayed accepted results in addition to their resolution values and the structure of their native co-crystallized ligands. Moreover, **Table 1** shows a description of the enumerated ligand features during the first step of the receptor-ligand pharmacophore generation procedure, the features

that matched the receptor-ligand interactions, and the number of pharmacophores generated from each crystal structure during the receptor-ligand pharmacophore generation step. Additionally, **Table 2** shows a description of the 111 pharmacophores generated in addition to their validation results in the ROC analysis procedure, i.e. (Number of true positives, Number of true negatives, Number of true positives, Number of true negatives, Sensitivity and Specificity).

### 2.3 Assessing the Validity of the resulted pharmacophores

In each pharmacophore generation run the resulting pharmacophores were directly graded according to their ROC performance and their GFA model results

#### 2.3.1 Receiver Operating Characteristic (ROC) Curve

ROC analysis aims towards analyzing the ability of a particular pharmacophore to sort a total list of already known actives and in-actives into their correct classes. The ROC performance is usually illustrated by the area under the curve (AUC) of the corresponding ROC along with other parameters such as: No. of true positives, No. of true negatives, No. of false positives, No. of false negatives, Sensitivity and specificity.<sup>12-14</sup>

**Table 2** shows the ROC analysis results of our selected passed pharmacophores. Figures 1A and 1B show the ROC curve of the pharmacophores with best ROC results (i.e.: Hypo **1XWS-2-4** (AUC value of 77.0 %), Hypo **2BIK-2-6** (AUC value of 74.3 %), Hypo **1XWS-2-6** (AUC value of 74.1 %), Hypo **3DCV-2-3** (AUC value of 71.1 %), Hypo **3BGZ-2-3** (AUC value of 71.2 %), Hypo **3DCV** (AUC value of 71.10 %), and Hypo **2BIK-2-7** (AUC value of 70.0 %)).

The fair results of ROC curves are attributed to the fact that the AUC calculation method during the ROC analysis process is dependent on the method used for curve fitting. ROC-AUC does not account for occurrence or different misclassification costs coming from false-negative and false-positive analyses;<sup>15</sup> meaning that using the pharmacophore mapping procedure in the early steps of ROC analysis to identify the actives from the in-actives does not in some cases give the right results. For example, in this case; the pharmacophore mapping procedure in DS 4.5 doesn't take into account the Pi-anion interactions (Anion- $\pi$  interactions are defined as favorable non-covalent contacts between electron-rich anions and

electron-deficient aromatic systems ( $\pi$ -acid)). This means that some truly active Pim-1 kinase inhibitors will be falsely un-mapped in the very early steps of the ROC analysis and so, all the later results will be in some way undervalued since some truly active pim-1 kinase inhibitors were excluded during the early steps of ROC analysis procedure. For this reason, this explanation encouraged us to accept the fairly good ROC analysis results and to use the DS.4.5 built in GFA model as an additional method to support our pharmacophore validation procedure.

### 2.3.2 DS.4.5 built in GFA model designed to score the resulted pharmacophores for the selectivity depending on the features and the 3D locations

The GFA model has an excellent prediction power for pharmacophoric selectivity, each pharmacophore resulted from the receptor-ligand pharmacophore generation step is validated according to the selectivity score based on a predictive model that uses simple descriptors derived from the type and relative location of the pharmacophore features to predict the number of hits from a diverse database,<sup>16</sup> (please refer to the experimental part: 4.1.5.2 : DS.4.5 built-in GFA validation model).

As we mentioned previously we used both the AUC-ROC curve criteria and the GFA selectivity score to choose the best pharmacophores that can specifically describe the inhibitory binding interactions inside the binding pocket of Pim-1 kinase. **Table 3** displays the success criteria of the superior pharmacophoric hypotheses in terms of both GFA selectivity and ROC-AUC validation procedures. The bolded pharmacophores are the ones that attained the best validation criteria among all the resulted 111 pharmacophores. **Table 4** shows the pharmacophoric features and corresponding weights, tolerances and 3D coordinates of successful selected pharmacophores: (Hypo **2BIK-2-6** (GFA selectivity value of 9.07), Hypo **1XWS-2-6** (GFA selectivity value of 9.07), Hypo **1XWS-2-4** (GFA selectivity value of 9.98), Hypo **3DCV-2-3** (GFA selectivity value of 9.50), Hypo **3BGZ-2-3** (GFA selectivity value of 5.95), Hypo **2BIK-2-7** (GFA selectivity value of 8.59) and Hypo **3DCV-2-10** (GFA selectivity value of 7.98). And finally, **Figures 2 and 3** summarize all pharmacophore extraction processes from each successful crystal ligand, and show the structural features of every successful pharmacophore.

## 2.4 Pharmacophore-Guided Synthesis of Novel Pim-1 kinase inhibitors

By comparing the features of pharmacophores, Hypo **1XWS\_2\_04**, Hypo **1XWS\_2\_06**, and Hypo **2BIK\_2\_06** (ROC AUC value of: 0.770, 0.743 and 0.741 respectively) (Figures: 2C, 2F, and 2I) with the other less superior pharmacophores (Figures: 2L, 3C, 3F, and 3I), we realized that the positively charged pharmacophoric feature that appeared seldom in the most superior pharmacophores is of a special value during the Pim-1 kinase inhibitory interaction inside the binding pocket of Pim-1 kinase. And by further analysis of the Pim-1 kinase binding pocket we concluded that the positively charged feature corresponds to the interaction between the positively charged ligand and the amino acids **Asp128** and **Asp131** in the hinge region extension part of Pim-1 kinase binding pocket. This conclusion has prompted us to synthesize an electron deficient Quinolone core that is able to confirm anion- $\pi$  interactions with the matching Aspartic acid moieties (**Asp128** and **Asp131**) (Please refer to **Figure 4** which shows detailed perspective about the important interactions inside this binding pocket of Pim-1 kinase).<sup>10</sup>

Anion- $\pi$  interactions are defined as favorable non-covalent contacts between electron-rich anions and electron-deficient aromatic systems ( $\pi$ -acid). Designing an electron deficient core for Pim-1 kinase inhibitors will confirm positive-negative interactions in the newly designed molecules without the need to steer the positive charge for a definite location and coordinate.<sup>17-19</sup> Furthermore, we integrated a carboxylic acid moiety at position number 3 of the Quinolone core to enhance the hydrogen bonding interaction in this region in order to assure the inhibitory effect of the ligands.

Additionally, the promising parameters of pharmacophores (Hypo **1XWS-2-4**, Hypo **1XWS-2-6**, Hypo **2BIK-2-6**, Hypo **2BIK-2-7**, Hypo **3BGZ-2-3**, Hypo **3DCV-2-3**, and Hypo **3DCV-2-10**) (Figures 2C, 2F, 2I, 2L, 3C, 3F, and 3I respectively) regarding their ROC and GFA performances encouraged us to engage them as templates to design novel Pim-1 kinase inhibitors which led us to envisage 6-fluoro-4-oxo-1,4-dihydro-quinoline-3-carboxylic acid based analogues as potential Pim-1 kinase inhibitors (Please refer to **Figure 5** which shows

the major synthons used to synthesize new inhibitors against Pim-1 kinase). Also, refer to **Figure 6** which shows designed compound **39-B** (8-amino-7-((2-carboxypropyl)amino)-6-fluoro-1-(4-fluorophenyl)-4-oxo-1,4-dihydroquinoline-3-carboxylic acid) mapped against: Hypo **2BIK-2-6**, Hypo **1XWS-2-6**, Hypo **3DCV-2-3**, Hypo **3BGZ-2-3**, Hypo **2BIK-2-7**, and Hypo **3DCV-2-10**. The 6-fluoro, 4-oxo, 3-carboxylic substitutions are considered electron withdrawing deactivating groups that can confer the Quinolone core even more electronically deficient and able to attract the nearby negatively charged Aspartic acid via an ionic Anion- $\pi$  interactions.

Accordingly, we can say that the 6-fluoro-4-oxo-1,4-dihydro-quinoline-3-carboxylic acid synthons (**Figure 5**) combine two advantages: (I) Simplistic synthesis method, and (II) approachability to wide-ranging functionalization required to accomplish the feature-rich nature of the successful pharmacophores. (Hypo **1XWS-2-4**, Hypo **1XWS-2-6**, Hypo **2BIK-2-6**, Hypo **2BIK-2-7**, Hypo **3BGZ-2-3**, Hypo **3DCV-2-3**, and Hypo **3DCV-2-10**) (Figures 2C, 2F, 2I, 2L, 3C, 3F, and 3I respectively).

Consequently, we prepared 6 Quinolone-based analogues (**Table 5**), Synthesis proceeded via nucleophilic aromatic replacements of chloro substituents on synthons A, B, C, and D (Figure 5) by  $\beta$ -alanine, DL- Aspartic acid, or isomethyl  $\beta$ -alanine, as outlined in **Schemes 1 and 2**. The synthesized compounds were tested their bioactivities. **Table 5** shows the synthesized hit molecules with their docking scoring function values against Pim-1 kinase (PDB code: 3BGZ, resolution 2.4 Å).

### 2.5 Comparison of Quinolone-based analogues with the active site of Pim-1 kinase

Quinolone-based analogues were further emphasized through their analogy within the binding pocket of Pim-1 kinase, i.e., upon analyzing the features of compound **40-B** (Table 5) and how it docks within Pim-1 kinase (PDB code: **1XWS**, resolution 1.8 Å), as in figure 7.

Particularly, The Para substituted halogen phenyl group at nitrogen number 1 of the Quinolone backbone (Please see compounds **38**, **39-B**, and **40-B** in table 5); undergoes clear Van der Waals interactions in the binding pocket of Pim-1 kinase mainly with the amino acid residue Leucine 44 (**Leu44**), Please See figure 7C which illustrates the hydrophobic

interactions between compound **40-B** and the binding pocket of Pim-1 kinase). On the other side, the 7-ethylamino side chain was also added to the Quinolone back bone and this also matches more hydrophobic interactions in the successful pharmacophores and the binding pocket of Pim- kinase (please refer to figure 7B to see the fitting between the ethyl amino group in compound **40-B** and the hydrophobic feature in pharmacophore Hypo **1XWS-2-6**). Then also, (refer to figure 7C and 7F to see the hydrophobic interaction between the docked compound **40-B** and the amino acid Valine 126 (**Val 126**)).

Mapping the Quinolone core of the newly synthesized ligands against PosIon feature in Hypo **1XWS\_2\_04**, Hypo **1XWS\_2\_06**, and Hypo **2BIK\_2\_06** (Figure 7B) corresponds to electrostatic attraction interactions tying the Quinolone electron deficient core with the carboxylic acid of **Asp131** (Figure 7A, 7D, 7E, and 7F). Similarly, mapping the carboxylic acid at position number 3 of the ligand's Quinolone core against hydrogen bond acceptor feature in Hypo **1XWS\_2\_06** (figure 7B) corresponds to conventional hydrogen bond interactions involving this hydrogen bond acceptor group with the side chain of **Asp121** (figures 7A, 7D, 7E, and 7F). Also, 7-ethylamino and 8-amino groups in compounds **39-B** and **40-B** satisfy the hydrogen bond donor functionality in Hypo **3DCV-2-3**, Hypo **2BIK-2-7** and Hypo **3DCV-2-10** (please refer to figures 6C, 6E, and 6F). Meanwhile, the oxy group on the quinolone back bone satisfy the hydrogen bond acceptor functionality in Hypo **2BIK-2-6**, Hypo **1XWS-2-6**, Hypo **3BGZ-2-3**, and Hypo **2BIK-2-7** (Please refer to figures 6A, 6B, 6D, and 6 E).

## 2.6 *In vitro* Evaluation for the synthesized compounds

The synthesized pure compounds were evaluated *in vitro* against human recombinant Pim-1 kinase assay kit (Cyclex®, Japan). These compounds were further assessed to determine their  $IC_{50}$  values. Our six compounds exhibited measurable anti-Pim-1 kinase bioactivities therefore they were evaluated to determine their  $IC_{50}$  values. Figure L under supplementary material illustrates the dose/response plots of the active hits.

Table 5 shows the active hits (**35-40**) and their measured in-vitro activities. Figure 7 shows the most active hit **40-B** ( $IC_{50} = 0.2950 \mu M$ ) docked into the binding pocket of Pim-1

kinase (PDB code: **1XWS**, resolution 1.8 Å) and by referring to this figure it is very clear that the 6-fluoro-4-oxo-1,4-dihydro-quinoline-3-carboxylic acid backbone confers very important contacts with **Asp128** and **Asp131** through the Anion- $\pi$  interactions and this result matches very well our first assumptions. In addition to that the **Val 126** which is part of the hinge region <sup>1</sup> binds via Fluorine hydrogen bonding with the Fluorine atom at position number 6 on the Quinolone core. All our synthesized compounds share the same Quinolone core please refer to table 6 for the Alignment and similarity analysis between our synthesized compounds.

Unexpectedly, upon performing the docking experiment on compound **39-B** ( $IC_{50}$  = 3.335  $\mu$ M) into the binding pocket of Pim-1 kinase crystal structure **1XWS** no results were achieved although the structure of compound **39-B** and compound **40-B** are very similar; compound **39-B** is 8-amino-7-((2-carboxyethyl)amino)-1-(4-fluorophenyl)-6-fluoro-4-oxo-1,4-dihydroquinoline-3-carboxylic acid (Table 5). Meanwhile, compound **40-B** is 8-amino-7-((2-carboxypropyl)amino)-6-fluoro-1-(4-chlorophenyl)-4-oxo-1,4-dihydroquinoline-3-carboxylic acid (Table 5, Figure 7). Docking compound **39-B** into the crystal structure of Pim-1 kinase (PDB code: **3DCV**, resolution 2.7 Å) (Figure 8) revealed very different binding mode for this compound. Actually, it seems that compound **39-B** flips upside down inside the binding pocket of Pim-1 kinase (Please see figure 8A which shows the binding mode of compound **39-B** inside the Pim-1 kinase binding pocket).

The Fluorine atom located at the para position of the phenyl group on the 6-fluoro-4-oxo-1,4-dihydroquinoline backbone in compound **39-B** (Table 5) acts as a hydrogen bond acceptor, this fact has been published and approved by Murray-Rust et al in 1983.<sup>20</sup> The Fluorine directed favorable interaction positions compound **39-B** inside the binding pocket of Pim- kinase so that the **Asp131** is away from the Quinolone core. Accordingly, the **Asp131** will have two kinds of interactions with the Fluorine-phenyl group: (i) Halogen hydrogen bonding interaction with Fluorine atom. (ii) Pi-Anion interaction with the electron deficient phenyl group. (Please refer to figures 8A - 8 F, that show 2D and 3D illustration of these interactions).

Our previous analysis that focuses on the different binding modes of compounds **39-B** and **40-B** inside the binding pocket of Pim-1 kinase explains the difference in their in vitro inhibitory activity against Pim-1 kinase, the  $IC_{50}$  value for compound **39-B** is 3.335  $\mu$ M meanwhile, the  $IC_{50}$  value for compound **40-B** is 0.2950  $\mu$ M. Moreover, compound **38** (Table 5) which also holds the Fluorine-phenyl substituent on its structure exhibits similar in vitro activity to compound **39-B** ( $IC_{50}$  value of 3.387  $\mu$ M, Table 5). Compounds **35** and **36** (Table 5) exhibits inferior anti-pim-1 kinase activity and this can be explained by the short side chains that are attached to the nitrogen number 1 on the Quinolone core of these compounds. Finally, compound **37** exhibits good anti-Pim-1 activity ( $IC_{50}$  value of 2.124  $\mu$ M, Table 5) although it holds a short side chain on the nitrogen number 1, and this can be explained by the internal lactonization on the ethyl amine side chain that might happen to this compound under physiological pH which might lead to new binding mode for this compound inside the binding pocket of Pim-1 kinase.

### 3.0 Conclusion

Our structure based receptor-ligand drug design of Pim-1 kinase proteins revealed unanticipated mode of recognition in the peri-hinge area of Pim-1 kinase. Unlike other kinases, Pim-1 kinases possess a hinge region which creates a unique binding pocket for ATP. Crystal structures of the Pim-1 kinase has been reported by more than a few labs.<sup>1</sup> And we have exploited the binding mode of these crystal structures and their co-crystallized ligands to anticipate and design new Pim-1 kinase inhibitors. In our previous ligand based study we showed that electron rich polycyclic structure is needed to interact with **Ile185, Val 52, Lys 67** (Figure 4). And now our structure based drug design revealed that electron deficient aromatic system is important to anchor pim-1 kinase inhibitors at this site of **Asp128** and **Asp131** through Pi-anion interactions (Figure 4). 111 pharmacophores resulted with acceptable ROC performance; **1XWS\_2\_04**, **2BIK\_2\_06** and **1XWS\_2\_06** (ROC AUC value of: 0.770, 0.743 and 0.741 respectively) were the best pharmacophores. These pharmacophores were employed to guide the synthesis of new series of 7-[(2-Carboxyethyl) amino]-1-substituted-6-fluoro-8-nitro-4-oxo-1,4-dihydro-quinoline-3-carboxylic acid and their reduced 8-amino derivatives which were later evaluated for their Pim-1 kinase inhibitory potencies. Of which the most potent illustrated an  $IC_{50}$  value of 0.29  $\mu$ M against Pim-1 kinase.

### Acknowledgments

This project was sponsored by the Deanship of Scientific Research in Zarqa University and the Deanship of Scientific Research in Hashemite University. The authors thank the Faculty of pharmaceutical sciences in Hashemite University for their generous help and support.

## 4. Experimental

### 4.1 Molecular modeling

#### 4.1.1 Computational software

The following software were applied:

- CS ChemDraw Ultra 6.0, Cambridge Soft Corp. (<http://www.cambridgesoft.com>), USA. 2D Structure drawing was performed employing.
- Discovery Studio 4.5 (DS 4.5) Standalone Applications, including **Catalyst** for analysis of pharmacophore data, **CHARM** for analyzing molecular simulation, **CNX** for 3D-structure determination and analysis of macromolecules, **MODLER** for analyzing protein structures, and **LigandFit** for molecular modeling and docking Biovia® ([www.3ds.com](http://www.3ds.com)), USA.
- Accelrys Enterprise Platform Server (**AEP**) ([www.3ds.com](http://www.3ds.com)), USA
- . The crystal structures of Pim-1 kinases were obtained from the protein data bank (<http://www.rcsb.org/>)

#### 4.1.2 Literature survey and Pim 1 crystal structures search

Our first goal in this project was to gather as much information as possible about Pim-1 kinase as a drug design target and to satisfy this goal we explored the Chemical European Bioinformatics Database (**ChEMBL**, <https://www.ebi.ac.uk/chembl/>) for Pim-1 kinase. The information in (**ChEMBL**) revealed the target **CHEMBL2147** which is a single protein Serine/threonine Pim-1 kinase derived from Homo sapiens. **CHEMBL2147** showed 104 crystal structures of Pim-1 kinase in the Protein data bank (<http://www.rcsb.org/>) and all of these crystal structures were explored in next drug design steps (Please refer to SM-1 under supplementary material for the PDB codes of Pim-1 kinase crystal structures used in the modelling step).

### 4.1.3 Preparing proteins for modeling

All Pim-1 kinase crystal structures that were downloaded from PDB were prepared for modeling using the protocol "Prepare protein" implemented in DS 4.5<sup>16</sup> protein preparation step includes removal of alternate conformations, removal of hetero-atoms from a protein structure, adding hydrogens, correcting missing or incorrectly specified residues, detecting valency violations and correcting them by changing the bond type or changing the formal charge.

### 4.1.4 Generating receptor-ligand pharmacophores

Selective pharmacophoric models representing ligand-receptor interaction are derived from co-crystallized molecules and their surrounding amino acids were generated using the protocol "Receptor-ligand Pharmacophore Generation".<sup>16</sup> The procedure is briefed as in five steps:

**First step:** Enumeration of pharmacophoric features on the original crystalized ligand:

The original crystalized ligand is scanned within its binding pocket structure for distinctive pharmacophoric features. The pharmacophoric features that have been considered in this step were: Hydrogen Bond Donor/Acceptor (HBD/HBA), Hydrophobic (HYD), Positive/Negative Ionizable (PI/NI), and Ring Aromatic (RA).<sup>16</sup>

**Second step:** Identifying features in the crystalized protein that match the receptor-ligand interactions: The pharmacophoric features that match the receptor-ligand interactions are identified by tying Hydrogen Bond Donors/Acceptors in the crystalized ligand with their Bond Donors/Acceptors pairs in the surrounding amino acids within a distance of 3.0 Å. Unmatched hydrogen bonds in the already scanned ligand in step 1 will be removed.<sup>11</sup> On the other hand, hydrophobic features on the scanned ligand within 5.5<sup>11</sup> of the centroid of a hydrophobic residue ( Alanine (Ala), Cysteine (Cys), Isoleucine (Ile), Leucine (Leu), Methionine (Met), Phenylalanine (Phe), Valine (Val) will be retained. As for Positive/Negative Ionizable groups: If the charge interaction is within 5.6 Å<sup>11</sup>, the feature is retained. All others are removed. Finally, Ring Aromatic: Retained if the protein has an aromatic ring within 2.5 Å from the projection point of the RA on the ligand.<sup>16</sup>

**Third step:** Building the of pharmacophore models

During this step, the pharmacophores are assembled. To assure the selectivity of the pharmacophores the number of pharmacophoric features will be specified to range from four to six. If the total of matching features for a protein complex is much greater than six, then there may be too many candidates. The basic goal of building a pharmacophore model is to search for multiple ligands that can bind to the same receptor. Therefore, the model should be sensitive enough to find potential novel ligands that can bind to the protein. However, it needs to be selective so that the false positive candidates are avoided.<sup>16</sup>

**Fourth step:** Adding exclusion volumes or shape constraints

Exclusion volumes are added to the pharmacophoric models by default. Addition of the exclusion volumes is based on inserting the exclusion volumes in the pharmacophoric map where ever there are a residue atoms 4.1 to 5.0 Å away from the ligand. The excluded volumes are placed at the centroid of the atoms and the size is proportional to the number of atoms.

**Fifth step:** Ranking the pharmacophores and retaining the most selective ones.

Screening a small diverse 3D database, CapDiverse, which is distributed with DS 4.5 is used as a direct method for ranking the selectivity of the resulted pharmacophore. The greater the hits captured, the less selective the pharmacophore.

#### **4.1.5 Assessing the Validity of the resulted pharmacophores**

During the modeling process two DS 4.5 built-in optional validation methods were employed in order to sort the resulted pharmacophores according to their selectivity, specificity and predictivity. These two methods are: The Receiver Operating Characteristic (ROC) Curve Analysis and the DS.4.5 built in Genetic Function Algorithm (GFA) model designed to score the resulted pharmacophores for the selectivity depending on the features and the 3D locations. The validation score is based on a predictive model that uses simple descriptors derived from the type and relative location of the pharmacophore features to predict the number of hits from a diverse database

##### **5.1.5.1 Receiver Operating Characteristic (ROC) Curve**

ROC curve is used to indicate how often a model correctly identifies true positives and true negatives. This procedure is based upon challenging the resulted successful pharmacophores to

selectively identify diverse Pim-1 kinase active inhibitors from a big pool of large actives and similar decoys using the ROC examination protocol implemented in DS 4.5.

ROC analysis procedure delivers some success criteria for evaluation: (i) Area Under the Curve (AUC) of the corresponding ROC curve, (ii) Number of true positives (TP) (iii) Number of true negatives (TN) (iv) Number of false positive (FP) (v) Number of false negative (FN) (vi) specificity (Sp., true negative rate), (vii) sensitivity (Se., true positive rate)<sup>11, 14, 21</sup>.

Our test set is composed of 1030 decoy compounds and 25 previously known pim-1 kinase inhibitors<sup>12, 22-27</sup> (Please see Table A under supplementary material for the structures of Pim-1 kinase inhibitors utilized as actives in decoy list). This set was assembled using the protocol "Find Similar Molecules" in DS 4.5, i.e. the 25 Pim-1 active were used to find similar decoy compounds from the zinc library<sup>13</sup> the following 2D descriptors were applied during finding similar molecules step: molecular weight, number of hydrogen bond donors and acceptors, number of rotatable bonds, log p, number of rings count and others. lastly, both the active diverse inhibitors and the similar zinc decoy compounds were combined together to form the decoy testing set.

Later on, the testing set was screened by each resulted pharmacophore through employing the validation option in Receptor-Ligand Pharmacophore Generation protocol implemented in DS 4.5.

The ROC curve analysis describes the sensitivity (Se or true positive rate, Eq. (1) as a function of (1-Sp). Sp is defined as specificity or true negative rate (Eq. (2)).<sup>12-13</sup>

$$Se = \frac{\text{Number of Selected Actives}}{\text{Total Number of Actives}} = \frac{TP}{TP + FN} \dots\dots\dots (1)$$

$$Sp = \frac{\text{Number of Discarded Inactives}}{\text{Total Number of Inactives}} = \frac{TN}{TN + FP} \dots\dots\dots (2)$$

The success of a certain pharmacophore in selecting the active compounds and discarding the inactive ones can be judged from the Area under the ROC curve (AUC).<sup>13-14, 27</sup> In an ideal ROC curve an AUC value of 1 is attained; however, random distributions cause an AUC value of 0.5. Virtual screening that performs better than a random discrimination of actives and decoys retrieve an AUC value between 0.5 and 1, however an AUC value lower than 0.5 signifies the unfavorable case of a

virtual screening method that has a higher probability to assign the best scores to decoys than to actives.<sup>7, 13-14</sup>

#### 5.1.5.2 DS.4.5 built-in GFA validation model

DS.4.5 built-in Genetic Function Algorithm(GFA) model was used to score the resulted pharmacophores for the selectivity depending on the features and the 3D locations. Obviously, the total number of computed pharmacophore models can be quite large since the total number of matching features is already large. The ROC method for ranking the resulted pharmacophores in is not satisfactory when used alone. Therefore, a GFA model is used as a rule-based scoring function for the selectivity depending on the features and the 3D locations.<sup>16</sup>This GFA model is employed within the receptor-Ligand Pharmacophore Generation protocol when using the Database option of the Advanced Selectivity Scoring parameter.

The GFA model for predicting the selectivity of a pharmacophore was built from a training set of 1544 pharmacophore models, each with two to eight features. This set is used for searching a database of 5384 diverse, druglike molecules. The database consists of 3000 drug-like compounds randomly selected from the Bio info database (<http://bioinfo-pharma.u-strasbg.fr/bioinfo>) and 2390 selected from the CAP database. The drug-like criteria used were: molecular weight of 150-550 D, 0-15 rotatable bonds, 0-10 HBAs, 0-5 HBDs, fewer than three charged atoms, and Polar surface area less than 150 Å<sup>2</sup>.

The logarithmic values of the number of database search hits are used as the targets. The following log values are used for zero hits based on the number of features: Two to five features: log(0.3), Six features: log(0.1), Seven Features: log(0.03), and Eight features: log(0.01). The number of total features in the pharmacophore models and the feature-feature distance bin values are used as the descriptors for training the GFA model. The GFA model has excellent prediction for selectivity.

#### 4.2 Pharmacophore-Guided Synthesis of Novel Pim-1 kinase inhibitors

Our argument that pharmacophores: (Hypo **2BIK-2-6**, Hypo **1XWS-2-6**, Hypo **3DCV-2-3**, Hypo **3BGZ-2-3**, Hypo **2BIK-2-7** and Hypo **3DCV-2-1**) are of promising parameters regarding their ROC and GFA performances, encouraged us to engage them as templates for designing novel Pim-1 kinase inhibitors. The successful pharmacophores (Tables 2 & 3, Figures 2C, 2F, 2I, 2L, 3C, 3F, and 3I) were used as guiding maps to design new compounds with proposed good affinity towards the Pim-1 kinase binding site. Figure 6 show our designed compound **39-B** mapped against the successful pharmacophores (Hypo **2BIK-2-6**, Hypo **1XWS-2-6**, Hypo **3DCV-2-3**, Hypo **3BGZ-2-3**, Hypo **2BIK-2-7** and Hypo **3DCV-2-10**). Besides, since these pharmacophores were originally extracted from the Pim-1 kinase binding pocket by the "Receptor-ligand Pharmacophore Generation" method, we can assume that our newly designed compounds would exert acceptable affinity against the Pim-1 kinase binding pocket.

Furthermore, the fairly good ROC performance of pharmacophores Hypo **1XWS-2-6** and Hypo **2BIK-2-6**, (AUC values of 0.770 and 0.743 respectively) encouraged us to further investigate their structures (Figures 2C and 2I respectively) which exhibit three hydrophobic wings and extra positively ionizable group that is only found in these two distinctive pharmacophores. This prompted us to envisage quinolone-based analogues as potential Pim-1 kinase inhibitors. Electron withdrawing groups such as (halogen, nitro and oxo groups) were added to the quinolone back bone to confer it more electron deficient and able to match the positively ionized group in our superior pharmacophores through Anion- $\pi$  interactions. Accordingly, our newly designed 7-[(2-Carboxyethyl) amino]-1-substituted-6-fluoro-8-nitro-4-oxo-1,4-dihydro-quinoline-3-carboxylic acid derivatives and their reduced 8-amino analogues would have the accessibility to diverse functionalization necessary to satisfy the feature-rich nature of the successful pharmacophores as shown in figure 6 which shows designed compound **39-B** (8-amino-7-((2-carboxypropyl) amino)-6-fluoro-1-(4-fluorophenyl)-4-oxo-1,4-dihydroquinoline-3-carboxylic acid) mapped against: (A) Hypo **2BIK-2-6** (B) Hypo **1XWS-2-6** (C) Hypo **3DCV-2-3** (D) Hypo **3BGZ-2-3** (E) Hypo **2BIK-2-7** (F) Hypo **3DCV-2-10**.

### 4.3 Docking experiments confirming the pharmacophore guided synthesis of Quinolone-based derivatives

Figure 6 shows the preliminary possibilities for the structural mapping between our designed compounds and the successful pharmacophores resulted from the Receptor-ligand pharmacophore generation step. The pharmacophore mapping was not enough to represent the affinity of our compounds towards the binding pocket of Pim-1 kinase enzyme since we based our drug design process on the anion- $\pi$  interactions between the electron deficient quinolone-based back bone and the positively ionized group of the superior pharmacophores: Hypo **1XWS-2-6** and Hypo **2BIK-2-6**, but this interaction can't be mapped through simple ligand pharmacophore mapping procedure implemented in DS 4.5.

So, in order to inspect the fitting of our designed quinolone-based derivatives (Table 5) into the binding pocket of Pim 1 kinase and to visualize the proposed anion- $\pi$  interactions between the quinolone core and the amino acids located at the binding pocket of Pim-1 kinase, we docked our newly designed molecules using the ligandfit docking algorithm implemented in the DS 4.5 into the binding pocket of the successful Pim-1 kinase crystal structures, namely: (PDB code: 1XWS, resolution 1.8 Å),(PDB code: 2BIK, resolution 1.8 Å), (PDB code: 3BGZ, resolution 2.4 Å), and (PDB code: 3DCV, resolution 2.7 Å).

The Ligandfit docking experiments consist of two major steps.<sup>16, 28</sup> First: Specifying the region of the receptor to be used as the binding site and Second: Docking ligands to the specified site which itself consists of the following: site partition using the conformational ligand/site shape matching to select ligand conformations that are similar to the shape of site. This is followed by positioning the selected ligand conformation into the binding site and rigid body energy minimization of the candidate ligand pose/conformation using the DockScore energy function. Finally, pose-saving algorithm comparing the candidate pose with the other stored candidates to ensure that redundant (i.e., similar) poses are rejected.<sup>16, 28</sup>

Accordingly, we prepared 6 Quinolone-based analogues and tested their bioactivities against Pim 1 kinase. Table 5 shows the prepared compounds, their predicted docking scores.

#### 4.4 Synthesis of Quinolone derivatives

##### General Synthetic procedures

All chemicals, reagents and solvents were of analytical/ synthetic grade were purchased from Sigma-Aldrich and Acros. Nuclear magnetic resonance spectra (NMR) were recorded on Bruker, Avance DPX-300 spectrometer. Infra-red (IR) spectra were recorded using Shimadzu 8400F FT-IR spectrophotometer (KBr discs). Melting points (MP) were determined in open capillaries on a Stuart scientific electro-thermal melting point apparatus, and are uncorrected. High-resolution mass spectra (HRMS) were measured in positive or negative ion mode using electrospray ion trap (ESI) technique by collision induced dissociation on a Bruker APEX-4 (7 Tesla) instrument. Microanalyses were performed using EuroVector Elemental Analyser, model (EA3000 A), Jordan University. Mobile phase mixtures for TLC were: System (1): Chloroform: methanol: formic acid (CHCl<sub>3</sub>: MeOH: FA) (94: 5: 1); System (2): CHCl<sub>3</sub>: MeOH: FA (90: 10: 1); System (3): Hexane: Ethyl acetate (50:50); System (4): System (1): system (3) (50: 50).

The following abbreviations are used: singlet (s), doublet (d), triplet (t), doublet of doublet (dd), doublet of doublet of doublet (ddd), doublet of triplet (dt), multiplet (m), broad signal (brs); High resolution mass spectra were determined on a high-resolution Micro Q-Tof apparatus (CRMP, Université Blaise Pascal, Clermont-Ferrand, France) or on a Waters Q-Tof 2 apparatus (CRMPO, Université de Rennes, France). Chromatographic purifications were performed by column chromatography using 40–63 ml silica gel. Reactions were monitored by TLC using fluorescent silica gel plates (60 F254 from Merck).

##### 5.4.1 Synthesis of (7-Chloro-1-Alkyl-6-fluoro-8-nitro-4-oxo-1,4-dihydroquinoline-3-carboxylic acid) Analogues (35-40-B, Schemes 1 & 2):

Synthons A, B, C, and D Figure 5, were used as starting materials during the synthesis process. These synthons were previously reported in literature by (Al-Hiari et al., 2008)<sup>29</sup>, (Al-Hiari et al., 2014)<sup>30</sup>, and (Al-Hiari et al., 2015)<sup>31</sup> (Please refer to SM-2: Synthesis of Synthons A, B, C, and D and scheme A under supplementary material). The synthesis of novel C-7-substituted derivatives of 1-alkyl-6-fluoro-8-nitro-4-oxo-1,4-dihydroquinoline-3-carboxylic acid was proceeded via nucleophilic aromatic

replacements of chloro substituents on Synthons A, B, C, and D (Figure 5) by  $\beta$ -alanine, DL- Aspartic acid, or isomethyl  $\beta$ -alanine as outlined in **Scheme 1**.

**7-[(2-Carboxyethyl)amino]-1-cyclopropyl-6-fluoro-8-nitro-4-oxo-1,4-dihydro-quinoline-3-carboxylic acid (compound 35, Table 5, scheme 1)**

A stirred mixture of  $\beta$ -alanine (1.1 g, 12 mmol), synthon A (Figure 5) (1.0 g, 3 mmol) and sodium hydrogen carbonate (1.5 g, 18 mmol) in 50 % aqueous ethanol (140 mL) was heated at 70-80 °C for 6 days under reflux conditions. The mixture slowly developed a light yellow color that changed into bright yellow, then into clear orange solution. The progress of the reaction was monitored by TLC, and was completed within 6 days. The mixture was extracted with dichloromethane (2 x 50 mL). The aqueous layer was cooled, its pH adjusted to 6-7 by addition of 3.5N HCl and extracted with  $\text{CH}_2\text{Cl}_2$  (50mL). Further acidification of the leftover aqueous layer to pH = 1-2 gave the title compound as a yellowish solid which was collected by filtration, washed with cold water (2 x 10 mL), dried and recrystallized from a mixture of chloroform and ethanol (1:1,v/v).  $^1\text{H-NMR}$  (300MHz, DMSO-  $d_6$ ):  $\delta$  0.96 (m, 4H,  $\text{H}_2\text{-}2'/\text{H}_2\text{-}3'$ ), 2.61 (d,  $J=5.70$  Hz, 2H,  $\text{CH}_2\text{-COOH}$ ), 3.69 (m, 1H,  $\text{H-}1'$ ), 4.30 (m, 2H,  $\text{CH}_2\text{-NH}$ ), 7.20 (d,  $J=9.3$  Hz, 1H,  $\text{NH-CH}_2$ ), 8.06 (d,  $^3J_{\text{H-F}}=13.8$  Hz, 1H,  $\text{H-}5$ ), 8.76 (s, 1H,  $\text{H-}2$ ), 12.40 (br s, 1H,  $\text{CH}_2\text{-CO}_2\text{H}$ ), 14.52 (br s, 1H,  $\text{C(3)-CO}_2\text{H}$ );  $^{13}\text{C-NMR}$  (300MHz, DMSO,  $d_6$ ):  $\delta$  10.13 ( $\text{C-}2'/\text{C-}3'$ ), 40.55 ( $\text{C-}1'$ ), 34.82( $\text{CH-CO}_2\text{H}$ ), 48.41 (d,  $^3J_{\text{C-F}}=14.1$  Hz,  $\text{CH}_2\text{-NH}$ ), 109.50 ( $\text{C-}3$ ), 114.73 (d,  $^2J_{\text{C-F}}=22.57$  Hz,  $\text{C-}5$ ), 116.74 (d,  $^3J_{\text{C-F}}=7.05$  Hz,  $\text{C-}4\text{a}$ ), 128.68 ( $\text{C-}8\text{a}$ ), 135.673 ( $\text{C-}8$ ), 138.71 (d,  $^2J_{\text{C-F}}=13.8$  Hz,  $\text{C-}7$ ), 150.55 (d,  $^1J_{\text{C-F}}=249$  Hz,  $\text{C-}6$ ), 152.15 ( $\text{C-}2$ ), 165.4 ( $\text{C(3)-CO}_2\text{H}$ ), 175.49 ( $\text{CH}_2\text{-CO}_2\text{H}$ ), 176.16 ( $\text{C-}4$ ); HRMS (ESI, -ve):  $m/z$  [ $\text{M-H}$ ]-  $\text{C}_{16}\text{H}_{13}\text{FN}_3\text{O}_7$  378.07430 requires: 378.07265.

**7-[(2-carboxyethyl)amino]-1-ethyl-6-fluoro-8-nitro-4-oxo-1,4-dihydroquinoline-3-carboxylic acid ( compound 36, Table 5, Scheme 1)<sup>29</sup>**

A stirred mixture of  $\beta$ -alanine (2.0 g, 22.5mmol), synthon B (Figure 5) ( 2.0 g, 6.3 mmol) and sodium hydrogen carbonate (3.0 g, 35.6 mmol) in 50 % aqueous ethanol (200 mL) was heated at 65-70 °C for 7-8 days under reflux conditions. The mixture slowly developed yellow color. The progress of the reaction was monitored by TLC, and was completed within 8 days. The mixture was extracted with dichloromethane (2 x 50 mL). The aqueous layer was cooled, its pH adjusted to 6-7 by addition of 3.5N HCl and re-extracted with  $\text{CH}_2\text{Cl}_2$  (50mL). Further acidification of the leftover aqueous layer to pH= 1-2 gave the title compound as yellowish solid which was collected by filtration, washed with cold water (2 x 10 mL), dried and recrystallized from a mixture of chloroform and ethanol (1:1, v/v);  $^1\text{H-NMR}$  (300MHz,  $\text{DMSO-}d_6$ ):  $\delta$  1.06 (t,  $J=6.9$  Hz, 3H,  $\text{CH}_2\text{CH}_3$ ), 2.57 (t,  $J = 6.5$  Hz, 2H,  $\text{CH}_2\text{-CO}_2\text{H}$ ), 3.70 (br t,  $J = 6.5$  Hz, 2H,  $\text{NH-CH}_2$ ), 4.1(q,  $J=7.2$ Hz, 2H,  $\text{CH}_2\text{CH}_3$ ), 7.96 (d,  $^3J_{\text{H-F}} = 11.7$  Hz, 1H, H-5), 7.65 (br s, 1H, NH), 8.58 (s, 1H, H-2);  $^{13}\text{C-NMR}$  (300MHz,  $\text{DMSO-}d_6$ ):  $\delta$  16.03 ( $\text{CH}_3$ ), 29.43 ( $\text{CH}_2\text{-CO}_2\text{H}$ ), 42.89 ( $\text{CH}_2\text{-NH}$ ), 50.51 ( $\text{CH}_2$ ), 108.70 (C-3), 114.7 (d,  $^2J_{\text{C-F}} = 22.9$  Hz, C-5), 116.5 (d,  $^3J_{\text{C-F}} = 7.2$  Hz, C-4a), 128.3 (d,  $^3J_{\text{C-F}} = 5.5$  Hz, C-8), 135.7 (C-8a), 138.8 (d,  $^2J_{\text{C-F}} = 14.3$  Hz, C-7), 148.33 (C-2), 150.4 (d,  $^1J_{\text{C-F}} = 248$  Hz, C-6), 166.2 (C(3)- $\text{CO}_2\text{H}$ ), 169.4 ( $\text{CH}_2\text{CO}_2\text{H}$ ), 176.0 (d,  $^4J_{\text{C-F}} = 2.6$  Hz, C-4); HRMS (ESI, +ve):  $m/z$  [ $\text{M}^{++} \text{Na}$ ] 390.07  $\text{C}_{15}\text{H}_{14}\text{FN}_3\text{O}_7 \text{Na}$  requires: 390.07144.

### 2-[(3-carboxy-1-ethyl-6-fluoro-8-nitro-4-oxo-1,4-dihydroquinolin-7-yl) amino]succinic acid (compound 37, Table 5, Scheme 1)

A stirred mixture of DL- Aspartic acid (2.5 g, 24.0 mmol), synthon B (Figure 5) (2.0 g, 6.35 mmol) and sodium hydrogen carbonate (4.5 g, 53.6 mmol) in 50 % aqueous ethanol (200 mL) was heated at 70-80 °C for 6 days under reflux conditions. The mixture slowly developed bright yellow, then into clear orange solution. The progress of the reaction was monitored by TLC, and was completed within 8 days. The mixture was worked up as described for compound 36. The titled compound was collected as bright yellow solid;  $^1\text{H-NMR}$  (300MHz,  $\text{DMSO-}d_6$ ):  $\delta$  1.27 (t,  $J= 7.7$ , 3H,  $\text{CH}_2\text{CH}_3$ ), 2.95 (d, d, d,  $J = 5.1, 14.7, 10.2$  Hz, 2H,  $\text{CH}_2\text{-CO}_2\text{H}$ ), 4.10 (m, 2H,  $\text{CH}_2\text{CH}_3$ ), 4.85 (d, d,  $J= 5.0, 13.5$  Hz, 1H,  $\text{CH-NH}$ ), 7.47 (d,  $J = 8.7$  Hz, 1H, NH), 8.14 (d,  $^3J_{\text{H-F}} = 13.6$  Hz, 1H, H-5), 8.90 (s, 1H, H-2), 12.51-13.32 (2m, 2H, C-1"- $\text{COOH}$  and C(3)- $\text{COOH}$ ), 14.72 (brs, 1H, C-2"- $\text{COOH}$ );  $^{13}\text{C-NMR}$  (300MHz,  $\text{DMSO-}d_6$ ):  $\delta$  15.58 ( $\text{CH}_3$ ), 37.12 ( $\text{CH}_2\text{-CO}_2\text{H}$ ), 51.88 ( $\text{CH}_2\text{CH}_3$ ), 54.99 (d,  $J = 12.07$  Hz,  $\text{CH-NH}$ ), 109.8 (C-

3), 115.12 (d,  $^2J_{C-F} = 22.8$  Hz, C-5), 118.47 (d,  $^3J_{C-F} = 7.12$  Hz, C-4a), 129.35 (d,  $^3J_{C-F} = 5.17$  Hz, C-8), 133.45 (C-8a), 137.99 (d,  $^2J_{C-F} = 14.17$  Hz, C-7), 150.67 (d,  $^1J_{C-F} = 248.7$  Hz, C-6), 151.08 (C-2), 165.54 (C(3)-CO<sub>2</sub>H), 172.55 (C-1"-CO<sub>2</sub>H), 172.62 (C-2"-CO<sub>2</sub>H), 175.45 (d,  $^4J_{C-F} = 2.47$  Hz, C-4); HRMS (ESI, +ve): m/z [M+] 412.07 C<sub>16</sub>H<sub>15</sub>FN<sub>3</sub>O<sub>9</sub> requires: 412.07875.

**7-[(2-carboxyethyl)amino]-6-fluoro-1-(4-fluorophenyl)-8-nitro-4-oxo-1,4-dihydroquinoline-3-carboxylic acid (compound 38, Table 5, Scheme 1)**

A stirred mixture of β-alanine (2.1 g, 23.5 mmol), synthon D (Figure 5) (2.30 g, 6 mmol) and sodium hydrogen carbonate (3 g, 35.8 mmol) in 50 % aqueous ethanol (140 mL) was heated at 70-80 °C for 6 days under reflux conditions. The mixture slowly developed a light yellow color that changed into bright yellow, then into clear orange solution. The progress of the reaction was monitored by TLC, and was completed within 6 days. The mixture was extracted with dichloromethane (2 x 50 mL). The aqueous layer was cooled, its pH adjusted to 6-7 by addition of 3.5N HCl and re-extracted with CH<sub>2</sub>Cl<sub>2</sub> (50mL). Further acidification of the leftover aqueous layer to pH = 1-2 gave the title compound as a yellowish solid which was collected by filtration, washed with cold water (2 x 10 mL), dried and recrystallized from a mixture of chloroform and ethanol (1:1,v/v). Yield 2.0 g (76.6%); R<sub>f</sub> value in system (3) = 0.2; mp= 231.6–233 °C; <sup>1</sup>H-NMR(300MHz, DMSO, *d*<sub>6</sub>): δ 2.55 (m, 2H, CH<sub>2</sub>-COOH), 3.63 (br m, 2H, CH<sub>2</sub>-NH), 7.08(br t, 1H, NH-CH<sub>2</sub>), 7.36 (d, d, J= 8.5, 8.5 Hz, 2H, H-3'/ H-5'), 7.68 (d, d, d, J= 4.8 Hz, 3.7 Hz, 4.2 Hz, 2H, H-2'/ H-6'), 8.13 (d,  $^3J_{H-F} = 13.76$  Hz, 1H, H-5), 8.47 (s, 1H, H-2), 12.42 (br s, 1H, C(3)-CO<sub>2</sub>H), 14.67 (br s, 1H, CH<sub>2</sub>-CO<sub>2</sub>H); <sup>13</sup>C-NMR (300MHz, DMSO, *d*<sub>6</sub>): δ 35.19 (CH<sub>2</sub>-CO<sub>2</sub>H), 41.73 (CH<sub>2</sub>-NH), 109.39(C-3), 114.15 (d,  $^2J_{C-F} = 23.25$  Hz, C-5), 116.87 (C-8a), 116.89 (d,  $^2J_{C-F} = 23.24$  Hz, C-3'/ C-5'), 128.42 (C-4a), 128.86 (d,  $^3J_{C-F} = 9.0$  Hz, C-2'/ C-6'), 133.85 (C-8), 138.16 (C-1'), 138.41 (d,  $^2J_{C-F} = 14.6$  Hz, C-7), 150.76 (d,  $^1J_{C-F} = 248$  Hz, C-6), 152.01 (C-2), 162.26 (d,  $^1J_{C-F} = 242$  Hz, C-4'), 165.33 (C(3)-CO<sub>2</sub>H), 173.09 (CH<sub>2</sub>CO<sub>2</sub>H), 175.5 (C-4); HRMS (ESI, -ve): m/z [M-H]-432.06433C<sub>19</sub>H<sub>12</sub>F<sub>2</sub>N<sub>3</sub>O<sub>7</sub> requires 432.06488.

**7-[(2-carboxypropyl)amino]- 1-(4-fluorophenyl)-6-fluoro-8-nitro-4-oxo-1,4-dihydroquinoline-3-carboxylic acid (compound 39-A, Scheme 1)**

A stirred mixture of isomethyl  $\beta$ -alanine (1.27 g, 12 mmol), synthon D (Figure 5) (1 g, 2.6 mmol) and sodium hydrogen carbonate (1.5 g, 18 mmol) in 50 % aqueous ethanol (140 mL) was heated at 70-80 °C under reflux conditions. The mixture slowly developed a light yellow color that changed into bright yellow, then into clear orange solution. The progress of the reaction was monitored by TLC, and was completed within 8 days. The mixture was worked up as described for compound 35. The titled compound was collected as bright yellow solid; <sup>1</sup>H-NMR (300MHz, DMSO-d<sub>6</sub>):  $\delta$  1.02 (d, J = 6.76 Hz, CH<sub>3</sub>), 2.72 (m, 1H, CH-COOH), 3.25 (m, 2H, CH<sub>2</sub>-NH), 7.18 (br t, J = 2.43 Hz, 1H, NH-CH<sub>2</sub>), 7.36 (d, d, J=8.1, 8.3 Hz, 2H, H-3'/ H-5'), 7.67 (m, 2H, H-2'/ H-6'), 8.13 (d, <sub>3</sub>J<sub>H-F</sub> = 14.1 Hz, 1H, H-5), 8.49 (s, 1H, H-2), 12.31 (br s, 1H, (C(3)-CO<sub>2</sub>H), 15.25 (br s, 1H, CH<sub>2</sub>CO<sub>2</sub>H); <sup>13</sup>C-NMR (300MHz, DMSO- d<sub>6</sub>):  $\delta$  14.94 (CH<sub>3</sub>), 40.81 (CH-CO<sub>2</sub>H), 48.24 (CH<sub>2</sub>-NH), 109.39 (C-3), 114.18 (d, <sub>2</sub>J<sub>C-F</sub> = 23.85 Hz, C-5), 115.10 (C-8a), 116.89 (d, <sub>2</sub>J<sub>C-F</sub> = 23.32 Hz, C-3'/ C-5'), 119.94 (C-4a), 128.90 (d, <sub>3</sub>J<sub>C-F</sub> = 9.45 Hz, C-2'/ C-6'), 133.89 (C-8), 138.50 (d, <sub>2</sub>J<sub>C-F</sub> = 17.8 Hz, C-7), 145.05 (C-1'), 151.25 (d, <sub>1</sub>J<sub>C-F</sub> = 255 Hz, C-6), 152.01 (C-2), 162.50 (d, <sub>1</sub>J<sub>C-F</sub> = 225 Hz, C-4'), 165.50 (C(3)-CO<sub>2</sub>H), 175.08 (CH-CO<sub>2</sub>H), 175.12 (C-4).

**8-amino-7-[(2-carboxypropyl)amino]-6-fluoro-1-(4-fluorophenyl)-4-oxo-1,4-dihydroquinoline-3-carboxylic acid (39-B, Scheme 2)**

To a stirred solution of compound **39-A** (0.5 g, 1.1 mmol) and potassium carbonate (0.96 g, 7 mmol) in water (20 mL) was added dropwise an aqueous solution of sodium dithionite (2.0 g, 11.5 mmol) in water (15 mL). The reaction mixture was further stirred at rt for 2 hrs. Thereafter, the pH of the solution was adjusted to about 2. The precipitated product was filtered, washed with water, air-dried and recrystallized from acetone and ethanol (1:1, v/v) to furnish faint yellow crystals. <sup>1</sup>H-NMR (300MHz, DMSO- *d*<sub>6</sub>): δ 1.08(d, *J* = 6.77 Hz, 3H, CH<sub>3</sub>), 2.27 (m, 1H, CH-COOH), 3.10 (m, 2H, CH<sub>2</sub>-NH), 4.19 (brs, 2H, NH<sub>2</sub>), 5.12 (br s, 1H, NH-CH), 7.39-7.52 (m, 3H: d, 1H, <sup>3</sup>*J*<sub>H-F</sub> = 8.15 Hz, H-5 and 2H, H-3'/H-5'), 7.69 (m, 2H, H-2'/H-6'), 8.45 (s, 1H, H-2), 12.29 (br s, 1H, C(3)-CO<sub>2</sub>H), 15.15 (br s, 1H, CH<sub>2</sub>-CO<sub>2</sub>H); <sup>13</sup>C-NMR (300MHz, DMSO- *d*<sub>6</sub>): δ 15.36 (CH<sub>3</sub>), 40.24 (CH-CO<sub>2</sub>H), 48.65 (H-NH), 100.69 (d, <sup>2</sup>*J*<sub>C-F</sub> = 23.78 Hz, C-5), 106.37 (C-3), 117.06 (d, <sup>3</sup>*J*<sub>C-F</sub> = 23.1 Hz, C-3'/C-5'), 121.09 (C-4a), 126.45 (C-8a), 128.74 (d, <sup>2</sup>*J*<sub>C-F</sub> = 8.85 Hz, C-2'/C-6'), 130.24 (d, <sup>2</sup>*J*<sub>C-F</sub> = 16.5 Hz, C-7), 131.21 (C-8), 139.55 (C-1'), 150.84 (d, <sup>1</sup>*J*<sub>C-F</sub> = 255 Hz, C-6), 151.36 (C-2), 162.16 (d, <sup>1</sup>*J*<sub>C-F</sub> = 234 Hz, C-4), 166.31 (C(3)-CO<sub>2</sub>H), 176.85 (CH<sub>2</sub>CO<sub>2</sub>H), 177.69 (C-4); HRMS (ESI, +ve): *m/z* [M<sup>+</sup>] 418.11 C<sub>20</sub>H<sub>18</sub>F<sub>2</sub>N<sub>3</sub>O<sub>5</sub> requires: 418.11885.

### **7-(2-Carboxy-ethylamino)-1-(4-chloro-phenyl)-6-fluoro-8-nitro-4-oxo-1,4-dihydro-quinoline-3-carboxylic acid (40-A, Scheme 1)**

A stirred mixture of β-alanine (2.1 g, 23.5 mmol), Synthon C (2.0 g, 4.4mmol) and sodium hydrogen carbonate (3 g, 35.8 mmol) in 50 % aqueous ethanol (140 mL) was heated at 70-80 °C for 6 days under reflux conditions. The mixture slowly developed a light yellow color that changed into deep yellow. The progress of the reaction was monitored by TLC, and was completed within 6 days. The mixture was worked up as described for compound **35**.

<sup>1</sup>H-NMR (300 MHz, DMSO- *d*<sub>6</sub>): δ 2.28 (d, *J* = 8.1, 2H, CH<sub>2</sub>-COOH), 3.66 (m, 2H, CH<sub>2</sub>-NH), 7.51 (br t, *J* = 5.7 Hz, 1H, NH-CH<sub>2</sub>), 7.51-7.54 (m, 2H, H-3', H-5'), 7.61-7.67 (m, 2H, H-2', H-6'), 8.2 (H-5), 8.62 (s, 1H, H-2); <sup>13</sup>C-NMR (300MHz, DMSO- *d*<sub>6</sub>): δ 35.17 (CH<sub>2</sub>-CO<sub>2</sub>H), 41.84 (CH<sub>2</sub>-NH), 109.60 (C-3), 114.18 (C-5), 116.58 (C-4a), 127.7 (C-3'), 128.03 (C-5'), 128.48 (C-8), 129.10 (C-2), 129.55 (C-6'), 133.79 (C-8), 134.50 (C-4'), 138.72 (C-7), 151.33 (d, <sup>1</sup>*J*<sub>C-F</sub> = 303.7 Hz, C-6), 145.08 (C-1'), 150.37 (C-2), 165.27 (C(3)-CO<sub>2</sub>H), 173.11 (CH<sub>2</sub>CO<sub>2</sub>H), 177.36 (C-4); HRMS (ESI, -ve): *m/z* [M<sup>-</sup>] 448.04 C<sub>19</sub>H<sub>12</sub>ClFN<sub>3</sub>O<sub>7</sub> requires 448.0353

**8-Amino-7-(2-carboxy-ethylamino)-1-(4-chloro-phenyl)-6-fluoro-4-oxo-1,4-dihydro-quinoline-3-carboxylic acid (40-B , Table 5, Scheme 2)**

To a stirred solution of compound **40-A** (0.5 g, 1.19mmol) and potassium carbonate (0.96g, 7 mmol) in water (20 mL) was added dropwise an aqueous solution of sodium dithionite (2.0 g, 11.5 mmol) in water (15 mL). The reaction mixture was further stirred at rt for 2 hrs. Thereafter, the pH of the solution was adjusted to about 2. The precipitated product was filtered, washed with water, air-dried and recrystallized from acetone and ethanol (1:1, v/v) to furnish faint yellow crystals.; <sup>1</sup>H-NMR (300MHz, DMSO- d<sub>6</sub>): δ 2.37 (m, 2H, CH<sub>2</sub>-COOH), 3.68 (m, 2H, CH<sub>2</sub>-NH), 5.05 ( brs, 2H, NH<sub>2</sub> ), 6.01 ( d, 1H, J = 7.29 Hz, CH<sub>2</sub>-NH), 7.42 -7.78 (m, 4H, H-3'/ H-5', H-2'/ H-6'), 8.45 (d,1H, <sup>3</sup>J<sub>H-F</sub>=8.08, H-5), 8.61 (s, 1H, H-2), 13.6 (br s, 1H, C(3)-CO<sub>2</sub>H), 15.2 (br s, 1H, CH<sub>2</sub>-CO<sub>2</sub>H); <sup>13</sup>C-NMR (300MHz, DMSO- d<sub>6</sub>):δ 35.08 (CH-CO<sub>2</sub>H),41.97 (CH<sub>2</sub>-NH ), 100.12 (C-5), 106.23 (C-3),130.18 (d, C-2'/C-6'), 119.185 (C-4a), 123.50 (C-8a), 128.76 (d, C-3'/C-5'), 126.69 (C-7), 132.62(C-8), 134.699(C-4'),141.60(C-1'),153.15(d, <sup>1</sup>J<sub>C-F</sub> = 285.6 Hz, C-6), 150.85 (C-2),166.25 (C(3)-CO<sub>2</sub>H),173.97 (CH<sub>2</sub>CO<sub>2</sub>H),177.78(C-4);HRMS (ESI, +ve): m/z [M+] 420.07 C<sub>19</sub>H<sub>16</sub>ClFN<sub>3</sub>O<sub>5</sub>requires: 420.07462.

#### 4.5 In Vitro Assay

##### 4.5.1 Materials

Pharmaceutical grade reagents and chemical materials were purchased from commercial vendors. Pim-1 kinase assay kit was purchased from Cyclex® Japan; solvents for bioanalysis were all purchased from Sigma-Aldrich (USA).

##### 4.5.2 Preparation of synthesized Compounds for In vitro Assay

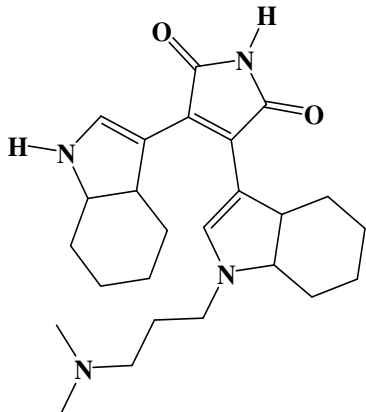
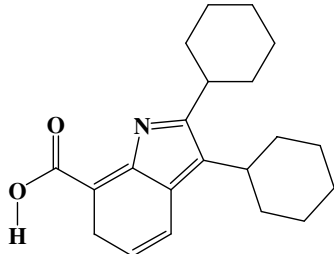
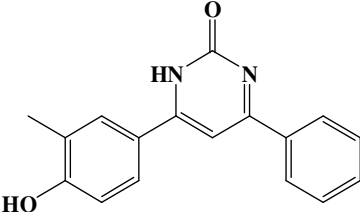
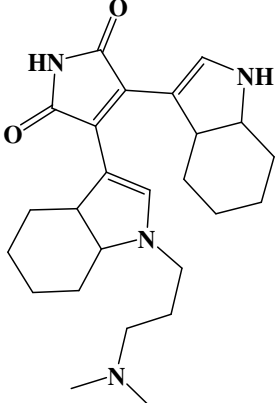
Powdered synthesized compounds to be tested (3.5 mg to 10 mg) were primarily dissolved in DMSO to give stock solutions of fixed concentrations. Then, they were diluted to the required concentrations with deionized water for in vitro assay evaluation.

##### 4.5.3 Spectrophotometric Assay of Pim-1 Kinase Inhibitors

Pim-1 kinase drug discovery kit Cyclex® (Japan) is composed of ELISA pre-coated 96 well plates with "recombinant p21waf1" antibody which can be selectively phosphorylated by Pim-1 kinase enzyme. A detector anti-phospho-p2waf1T145 polyclonal antibody is conjugated to horse radish peroxidase antibody PWT-01, and can explicitly detect the phosphorylated form of "recombinant p21waf1".

Upon performing the assay hits to be tested are first diluted with the kinase buffer. Afterwards, the hits' solutions are pipetted into pre-coated 96 well plates to yield final concentrations of 0.1, 1.0, and 10  $\mu$ M. Then, Pim-1 kinase was added to each well as aqueous solution 0.01 units in 10  $\mu$ L, and allowed to phosphorylate the bound substrate in the presence of ATP natural kinase substrate. The amount of phosphorylated substrate was quantified by using the detector antibody conjugated to horse radish peroxidase which then catalyzes the change of chromogenic substrate tetra-methylbenzidine (TMB) from a colorless solution to a blue solution. The color of the solution is measured using Bio-Tek instruments (ELx 800 Winooski VT) spectrophotometric plate reader at a wavelength of 650 nm and the inhibition of Pim-1 kinase is calculated as percent activity of the uninhibited Pim-1 kinase enzyme control.

**Table 1:** Selected Pim-1 kinase crystals with their co-crystallized ligands and matching features

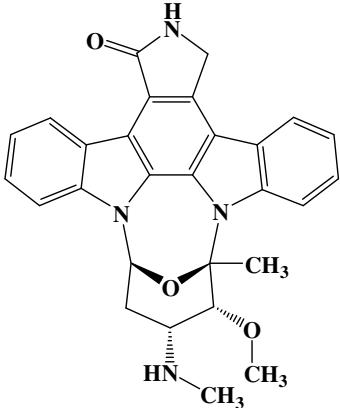
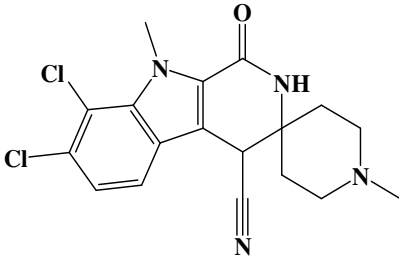
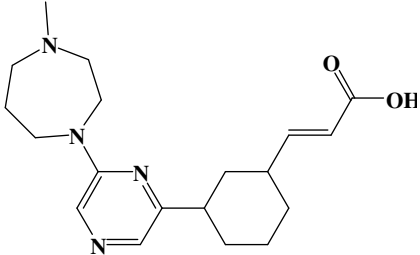
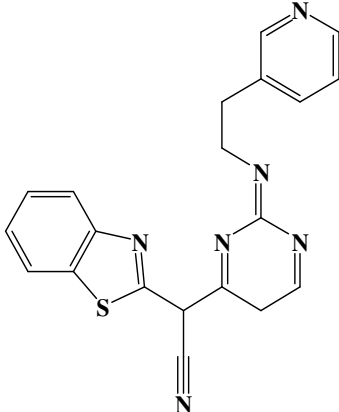
PDB code	Ligand	Res. <sup>a</sup>	No. of features in ligand	features match the receptor-ligand interactions:	No. of pharm . generated
2BIK <sup>b</sup> BII1306 <sup>c</sup>		1.8 Å	16	HBD, 3xHbic, RingArom, PosIon	10
3BGZ <sup>b</sup> VX3314		2.4 Å	13	3xHbic, 2xRingArom, NegIon	7
3DCV <sup>b</sup> 55E500		2.7 Å	16	HBA, 2xHBD, 2xHbic, RingArom	10
1XWS <sup>b</sup> BII1001		1.8 Å	16	HBA, HBD, 3xHbic, PosIon	10

<sup>a</sup>Corresponds to the resolution of the Pim-1 kinase specified crystal in the PDB.

<sup>b</sup>The PDB code for the crystal structure of Pim-1 kinase and below is the name of its co-crystallized ligand.

<sup>c</sup>The name of the co-crystallized ligand in the PDB

**Table 1:** Selected Pim-1 kinase crystals with their co-crystallized ligands and matching features

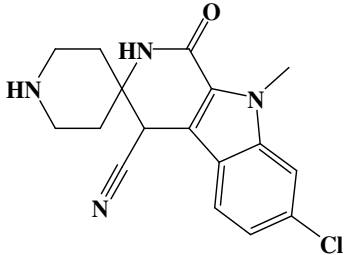
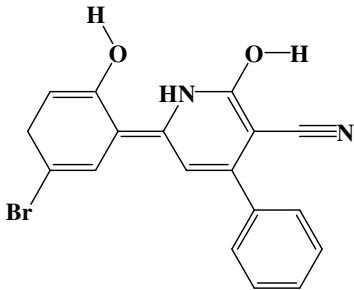
PDB code	Ligand	Res. <sup>a</sup>	No. of features in ligand	features match the receptor-ligand interactions:	No. of pharm. generated
1YHS <sup>b</sup> Staurosporine		2.15 Å	22	HBD, 4xHbic, PosIon	10
3CXW <sup>b</sup> 7CP501		2.1 Å	14	HBD, 4xHbic, PosIon	10
3F2A <sup>b</sup> MG314		1.9 Å	13	Hbic, 3xRingArom, PosIon, NegIon	7
3CY3 <sup>b</sup> JN5501		2.15 Å	15	HBA, HBD, 3xHbic, PosIon	7

<sup>a</sup>Corresponds to the resolution of the Pim-1 kinase specified crystal in the PDB.

<sup>b</sup>The PDB code for the crystal structure of Pim-1 kinase and below is the name of its co-crystallized ligand.

<sup>c</sup>The name of the co-crystallized ligand in the PDB.

**Table 1:** Selected Pim-1 kinase crystals with their co-crystallized ligands and matching features

PDB code	Ligand	Res. <sup>a</sup>	No. of features in ligand	features match the receptor-ligand interactions:	No. of pharm. generated
3CY2 <sup>b</sup> MB9501		2.01 Å	14	HBA, HBD, 3xHbic, PosIon	10
2OBJ <sup>b</sup> VRV400		2.5 Å	17	2xHBA, 2xHBD, 3xHbic	10

<sup>a</sup>Corresponds to the resolution of the Pim-1 kinase specified crystal in the PDB.

<sup>b</sup>The PDB code for the crystal structure of Pim-1 kinase and below is the name of its co-crystallized ligand.

<sup>c</sup>The name of the co-crystallized ligand in the PDB.

**Table 2:** Success criteria of the accepted pharmacophoric hypotheses

Pharm <sup>a</sup>	Features	Validation with known active/inactives							
		Actives <sup>b</sup>	Inactives <sup>c</sup>	TP <sup>d</sup>	TN <sup>e</sup>	FP <sup>f</sup>	FN <sup>g</sup>	Sens <sup>h</sup>	Specif. <sup>i</sup>
2BIK_2_01	HBA, HBD, 3xHbic, PosIon	25	1030	4	984	46	21	0.1600	0.9553
2BIK_2_02	HBA, HBD, 2xHbic, PosIon	25	1030	11	875	155	14	0.4400	0.8495
2BIK_2_03	HBA, HBD, 2xHbic, PosIon	25	1030	7	902	128	18	0.2800	0.8757
2BIK_2_04	HBD, 3xHbic, PosIon	25	1030	16	845	185	9	0.6400	0.8203
2BIK_2_05	HBA, HBD, 2xHbic, PosIon	25	1030	8	828	202	17	0.3200	0.8038
<b>2BIK_2_06</b>	<b>HBA, 3xHbic, PosIon</b>	<b>25</b>	<b>1030</b>	<b>18</b>	<b>729</b>	<b>301</b>	<b>7</b>	<b>0.7200</b>	<b>0.7077</b>
<b>2BIK_2_07</b>	<b>HBA, HBD, 3xHbic</b>	<b>25</b>	<b>1030</b>	<b>17</b>	<b>660</b>	<b>370</b>	<b>8</b>	<b>0.6800</b>	<b>0.6407</b>
2BIK_2_08	HBA, HBD, Hbic, PosIon	25	1030	15	671	359	10	0.6000	0.6514
2BIK_2_09	HBA, HBD, Hbic, PosIon	25	1030	16	580	450	9	0.6400	0.5631
2BIK_2_10	HBA, HBD, Hbic, PosIon	25	1030	4	719	311	21	0.1600	0.6980
3BGZ_2_01	3xHbic, NegIon	25	1030	16	468	562	9	0.6400	0.4543
3BGZ_2_02	3xHbic, 2x RingArom	25	1030	9	519	511	16	0.3600	0.5038
<b>3BGZ_2_03</b>	<b>3xHbic, RingArom</b>	<b>25</b>	<b>1030</b>	<b>24</b>	<b>195</b>	<b>835</b>	<b>1</b>	<b>0.9600</b>	<b>0.1893</b>
3BGZ_2_04	3xHbic, RingArom	25	1030	24	133	897	1	0.9600	0.1291
3BGZ_2_05	2xHbic, 2x RingArom	25	1030	17	215	815	8	0.6800	0.2087
3BGZ_2_06	2xHbic, 2x RingArom	25	1030	15	311	719	10	0.6000	0.3019
3BGZ_2_07	2xHbic, 2x RingArom	25	1030	23	187	843	2	0.9200	0.1815
3DCV_2_01	HBA, 2xHBD, 2xHbic, RingArom	25	1030	4	986	44	21	0.1600	0.9572
3DCV_2_02	HBA, 2xHBD, 2xHbic	25	1030	6	878	152	19	0.2400	0.8524
<b>3DCV_2_03</b>	<b>2xHBD, 2xHbic, RingArom</b>	<b>25</b>	<b>1030</b>	<b>13</b>	<b>900</b>	<b>130</b>	<b>12</b>	<b>0.5200</b>	<b>0.8737</b>
3DCV_2_04	HBA, 2xHBD, Hbic, RingArom	25	1030	2	881	149	23	0.0800	0.8553
3DCV_2_05	HBA, 2xHBD, Hbic, RingArom	25	1030	2	911	119	23	0.0800	0.8844
3DCV_2_06	HBA, HBD, 2xHbic, RingArom	25	1030	11	716	314	14	0.4400	0.6951
3DCV_2_07	HBA, HBD, 2xHbic, RingArom	25	1030	10	749	281	15	0.4000	0.7271
3DCV_2_08	2xHBD, Hbic, RingArom	25	1030	16	721	309	9	0.6400	0.7000
3DCV_2_09	2xHBD, Hbic, RingArom	25	1030	15	600	430	10	0.6000	0.5825
<b>3DCV_2_10</b>	<b>2xHBD, 2xHbic</b>	<b>25</b>	<b>1030</b>	<b>16</b>	<b>761</b>	<b>269</b>	<b>9</b>	<b>0.6400</b>	<b>0.7388</b>
1YHS_2_01	HBD, 4xHbic, PosIon	25	1030	6	999	31	19	0.5600	0.9699
1YHS_2_02	HBD, 3xHbic, PosIon	25	1030	14	885	145	11	0.5600	0.8592
1YHS_2_03	HBD, 3xHbic, PosIon	25	1030	15	845	185	10	0.6000	0.8203
1YHS_2_04	HBD, 3xHbic, PosIon	25	1030	4	921	109	21	0.1600	0.8941
1YHS_2_05	HBD, 3xHbic, PosIon	25	1030	11	838	192	14	0.4400	0.8135
1YHS_2_06	4xHbic, PosIon	25	1030	12	742	288	13	0.4800	0.7203
1YHS_2_07	HBD, 4xHbic	25	1030	13	735	295	12	0.5200	0.7135
1YHS_2_08	HBD, 2xHbic, PosIon	25	1030	19	546	484	6	0.7600	0.5301
1YHS_2_09	HBD, 2xHbic, PosIon	25	1030	14	696	334	11	0.5600	0.6757
1YHS_2_10	HBD, 2xHbic, PosIon	25	1030	12	700	330	13	0.4800	0.6796
3CXW_2_01	HBD, 4xHbic, PosIon	25	1030	0	988	42	25	0	0.95922
3CXW_2_02	HBD, 3xHbic, PosIon	25	1030	5	868	162	20	0.2000	0.8427
3CXW_2_03	HBD, 3xHbic, PosIon	25	1030	5	914	116	20	0.2000	0.8873
3CXW_2_04	HBD, 3xHbic, PosIon	25	1030	12	843	187	13	0.4800	0.8184
3CXW_2_05	HBD, 3xHbic, PosIon	25	1030	13	863	167	12	0.5200	0.8378
3CXW_2_06	4xHbic, PosIon	25	1030	5	894	136	20	0.2000	0.8679
3CXW_2_07	HBD, 4xHbic	25	1030	13	781	249	12	0.5200	0.7582
3CXW_2_08	HBD, 2xHbic, PosIon	25	1030	13	656	374	12	0.5200	0.6368
3CXW_2_09	HBD, 2xHbic, PosIon	25	1030	20	504	526	5	0.8000	0.4893
3CXW_2_10	HBD, 2xHbic, PosIon	25	1030	13	695	335	12	0.5200	0.6747

**Table 2:** Success criteria of the accepted pharmacophoric hypotheses

Pharm <sup>a</sup>	Features	Validation with known active/inactives							
		Actives <sup>b</sup>	Inactives <sup>c</sup>	TP <sup>d</sup>	TN <sup>e</sup>	FP <sup>f</sup>	FN <sup>g</sup>	Sens. <sup>h</sup>	Specif. <sup>i</sup>
1XWS_2_01	HBA, HBD, 3xHbic, PosIon	25	1030	3	968	62	22	0.1200	0.9398
1XWS_2_02	HBA, HBD, 2xHbic, PosIon	25	1030	12	875	155	13	0.4800	0.8495
1XWS_2_03	HBA, HBD, 2xHbic, PosIon	25	1030	9	880	150	16	0.3600	0.8543
1XWS_2_04	HBD, 3xHbic, PosIon	25	1030	17	847	183	8	0.6800	0.8223
1XWS_2_05	HBA, HBD, 2xHbic, PosIon	25	1030	11	819	211	14	0.4400	0.7951
<b>1XWS_2_06</b>	<b>HBA, 3xHbic, PosIon</b>	<b>25</b>	<b>1030</b>	<b>18</b>	<b>710</b>	<b>320</b>	<b>7</b>	<b>0.7200</b>	<b>0.6893</b>
1XWS_2_07	HBA, HBD, 3xHbic	25	1030	16	650	380	9	0.6400	0.6310
1XWS_2_08	HBA, HBD, Hbic, PosIon	25	1030	14	674	356	11	0.5600	0.6543
1XWS_2_09	HBA, HBD, Hbic, PosIon	25	1030	15	577	453	10	0.6000	0.5601
1XWS_2_10	HBA, HBD, Hbic, PosIon	25	1030	10	697	333	15	0.4000	0.6767
3F2A_2_01	HBA, Hbic, NegIon, PosIon	25	1030	16	604	426	9	0.6400	0.5864
3F2A_2_02	3xHBA, Hbic, PosIon	25	1030	6	838	192	19	0.2400	0.8135
3F2A_2_03	2xHBA, Hbic, PosIon	25	1030	15	372	658	10	0.6000	0.3611
3F2A_2_04	2xHBA, Hbic, PosIon	25	1030	18	378	652	7	0.7200	0.3669
3F2A_2_05	2xHBA, Hbic, PosIon	25	1030	22	286	744	3	0.8800	0.2776
3F2A_2_06	3xHBA, PosIon	25	1030	7	633	397	18	0.2800	0.6145
3F2A_2_07	2xHBA, Hbic	25	1030	7	399	631	18	0.2800	0.3873
3CY3_2_01	HBA, 3xHbic, PosIon	25	1030	13	693	337	12	0.5200	0.6728
3CY3_2_02	3xHbic, PosIon	25	1030	23	367	663	2	0.9200	0.3563
3CY3_2_03	HBA, 2xHbic, PosIon	25	1030	18	379	651	7	0.7200	0.3679
3CY3_2_04	HBA, 2xHbic, PosIon	25	1030	20	412	618	5	0.8000	0.4000
3CY3_2_05	HBA, 2xHbic, PosIon	25	1030	22	395	635	3	0.8800	0.3835
3CY3_2_06	HBA, HBD, 2xHbic	25	1030	19	417	613	6	0.7600	0.4048
3CY3_2_07	HBA, 3xHbic	25	1030	21	314	716	4	0.8400	0.3048
3CY2_2_01	HBA, HBD, 3xHbic, PosIon	25	1030	2	974	56	23	0.0800	0.9456
3CY2_2_02	HBA, HBD, 2xHbic, PosIon	25	1030	6	853	177	19	0.2400	0.8281
3CY2_2_03	HBA, HBD, 2xHbic, PosIon	25	1030	10	821	209	15	0.4000	0.7970
3CY2_2_04	HBD, 3xHbic, PosIon	25	1030	11	793	237	14	0.4400	0.7699
3CY2_2_05	HBA, HBD, 2xHbic, PosIon	25	1030	7	791	239	18	0.2800	0.7679
3CY2_2_06	HBA, 3xHbic, PosIon	25	1030	10	656	374	15	0.4000	0.6368
3CY2_2_07	HBA, HBD, 3xHbic	25	1030	15	609	421	10	0.6000	0.5912
3CY2_2_08	HBA, HBD, Hbic, PosIon	25	1030	9	679	351	16	0.3600	0.6592
3CY2_2_09	HBA, HBD, Hbic, PosIon	25	1030	9	675	355	16	0.3600	0.6553
3CY2_2_10	HBA, HBD, Hbic, PosIon	25	1030	13	563	467	12	0.5200	0.5466
2OBJ_2_01	2xHBD, 3xHbic	25	1030	8	821	209	17	0.3200	0.7970
2OBJ_2_02	HBA, HBD, 3xHbic	25	1030	12	553	477	13	0.4800	0.5368
2OBJ_2_03	HBA, HBD, 3xHbic	25	1030	16	660	370	9	0.6400	0.6407
2OBJ_2_04	2xHBD, 2xHbic	25	1030	15	603	427	10	0.6000	0.5854
2OBJ_2_05	2xHBD, 2xHbic	25	1030	17	689	341	8	0.6800	0.6689
2OBJ_2_06	2xHBD, 2xHbic	25	1030	16	478	552	9	0.6400	0.4640
2OBJ_2_07	2xHBA, 3xHbic	25	1030	18	339	691	7	0.7200	0.3291
2OBJ_2_08	HBA, HBD, 2xHbic	25	1030	16	318	712	9	0.6400	0.3087
2OBJ_2_09	HBA, HBD, 2xHbic	25	1030	17	488	542	8	0.6800	0.4737
2OBJ_2_10	HBA, HBD, 2xHbic	25	1030	23	227	803	2	0.9200	0.2203

**Table 2:** Success criteria of the accepted pharmacophoric hypotheses

Pharm <sup>a</sup>	Features	Validation with known active/inactives							
		Actives <sup>b</sup>	Inactives <sup>c</sup>	TP <sup>d</sup>	TN <sup>e</sup>	FP <sup>f</sup>	FN <sup>g</sup>	Sens. <sup>h</sup>	Specif. <sup>i</sup>
2O64_2_01	2xHBA, 3xHBD	25	1030	0	1027	3	25	0	0.9970
2O64_2_02	3xHBA, 2xHBD	25	1030	1	1004	26	24	0.0400	0.9747
2O64_2_03	3xHBA, 2xHBD	25	1030	0	1002	28	25	0	0.9728
2O64_2_04	HBA, 3xHBD	25	1030	1	995	35	24	0.0400	0.9660
2O64_2_05	HBA, 3xHBD	25	1030	3	994	36	22	0.1200	0.9650
2O64_2_06	4xHBA, HBD	25	1030	0	993	37	25	0	0.9640
2O64_2_07	2xHBA, 2xHBD	25	1030	3	919	111	22	0.1200	0.8922
2O64_2_08	2xHBA, 2xHBD	25	1030	1	918	112	24	0.0400	0.8912
2O64_2_09	2xHBA, 2xHBD	25	1030	2	920	110	23	0.0800	0.8932
2O64_2_10	2xHBA, 2xHBD	25	1030	1	939	91	24	0.0400	0.9116
3QF9_2_01	2xHBA, HBD, 3xHbic	25	1030	4	991	39	21	0.1600	0.9621
3QF9_2_02	2xHBA, HBD, 2xHbic	25	1030	6	897	133	19	0.2400	0.8708
3QF9_2_03	2xHBA, HBD, 2xHbic	25	1030	7	870	160	18	0.2800	0.8446
3QF9_2_04	2xHBA, HBD, 2xHbic	25	1030	5	892	138	20	0.2000	0.8660
3QF9_2_05	HBA, HBD, 3xHbic	25	1030	10	724	306	15	0.4000	0.7029
3QF9_2_06	HBA, HBD, 3xHbic	25	1030	7	788	242	18	0.2800	0.7650
3QF9_2_07	2xHBA, 3xHbic	25	1030	7	713	317	18	0.2800	0.6922
3QF9_2_08	2xHBA, HBD, Hbic	25	1030	11	746	284	14	0.4400	0.7242
3QF9_2_09	2xHBA, HBD, Hbic	25	1030	6	760	270	19	0.2400	0.7378
3QF9_2_10	2xHBA, HBD, Hbic	25	1030	15	724	306	10	0.6000	0.7029

<sup>a</sup>Correspond to pharmacophores resulted from the Receptor-Ligand Pharmacophore Generation run.

<sup>b</sup>Total actives in the tested decoy list

<sup>c</sup>TotalInactives in the tested decoy list

<sup>d</sup>Number of true positives.

<sup>e</sup>Number of true negatives.

<sup>f</sup>Number of false positive

<sup>g</sup> Number of false negative.

<sup>h</sup> Sensitivity

<sup>i</sup> Specificity

**Table 3:** Success criteria of the superior pharmacophoric hypotheses in both GFA selectivity and ROC-AUC validation steps.

Pharmacophore	No. of features	Features	GFA model Selectivity score <sup>a</sup>	ROC-AUC
1XWS_2_01	6	HBA, HBD, 3xHbic, PosIon	11.498	0.533
1XWS_2_02	5	HBA, HBD, 2xHbic, PosIon	9.9830	0.672
1XWS_2_03	5	HBA, HBD, 2xHbic, PosIon	9.9830	0.599
<b>1XWS_2_04</b>	<b>5</b>	<b>HBD, 3xHbic, PosIon</b>	<b>9.9830</b>	<b>0.770</b>
1XWS_2_05	5	HBA, HBD, 2xHbic, PosIon	9.9830	0.618
<b>1XWS_2_06</b>	<b>5</b>	<b>HBA, 3xHbic, PosIon</b>	<b>9.0695</b>	<b>0.741</b>
1XWS_2_07	5	HBA, HBD, 3xHbic	8.5895	0.689
1XWS_2_08	4	HBA, HBD, Hbic, PosIon	8.4682	0.618
1XWS_2_09	4	HBA, HBD, Hbic, PosIon	8.4682	0.638
1XWS_2_10	4	HBA, HBD, Hbic, PosIon	8.4682	0.508
2BIK_2_01	6	HBA, HBD, 3xHbic, PosIon	11.498	0.559
2BIK_2_02	5	HBA, HBD, 2xHbic, PosIon	9.9830	0.645
2BIK_2_03	5	HBA, HBD, 2xHbic, PosIon	9.9830	0.575
2BIK_2_05	5	HBA, HBD, 2xHbic, PosIon	9.9830	0.573
<b>2BIK_2_06</b>	<b>5</b>	<b>HBA, 3xHbic, PosIon</b>	<b>9.0695</b>	<b>0.743</b>
<b>2BIK_2_07</b>	<b>5</b>	<b>HBA, HBD, 3xHbic</b>	<b>8.5895</b>	<b>0.700</b>
2BIK_2_08	4	HBA, HBD, Hbic, PosIon	8.4682	0.627
2BIK_2_09	4	HBA, HBD, Hbic, PosIon	8.4682	0.636
2BIK_2_10	4	HBA, HBD, Hbic, PosIon	8.4682	0.595
3DCV_2_01	6	HBA, 2xHBD, 2xHbic,	11.018	0.560
3DCV_2_02	5	HBA, 2xHBD, 2xHbic	9.5030	0.555
<b>3DCV_2_03</b>	<b>5</b>	<b>2xHBD, 2xHbic, RingArom</b>	<b>9.5030</b>	<b>0.711</b>
3DCV_2_04	5	HBA, 2xHBD, Hbic, RingArom	9.5030	0.531
3DCV_2_05	5	HBA, 2xHBD, Hbic, RingArom	9.5030	0.516
3DCV_2_06	<b>5</b>	HBA, HBD, 2xHbic, RingArom	8.5895	0.568
3DCV_2_07	4	HBA, HBD, 2xHbic, RingArom	8.5895	0.578
3DCV_2_08	4	2xHBD, Hbic, RingArom	7.9882	0.685
3DCV_2_09	4	2xHBD, Hbic, RingArom	7.9882	0.611
<b>3DCV_2_10</b>	<b>6</b>	<b>2xHBD, 2xHbic</b>	<b>7.9882</b>	<b>0.711</b>
3BGZ_2_01	4	3xHbic, NegIon	8.1653	0.579
3BGZ_2_02	5	3xHbic, 2x RingArom	7.4702	0.584
<b>3BGZ_2_03</b>	<b>4</b>	<b>3xHbic, RingArom</b>	<b>5.9554</b>	<b>0.712</b>
3BGZ_2_04	4	3xHbic, RingArom	5.9554	0.659
3BGZ_2_05	4	2xHbic, 2x RingArom	5.9554	0.557
3BGZ_2_06	4	2xHbic, 2x RingArom	5.9554	0.537
3BGZ_2_07	4	2xHbic, 2x RingArom	5.9554	0.639

<sup>a</sup>selectivity score is based on a predictive GFA model that uses simple descriptors derived from the type and relative location of the pharmacophoric features to predict the number of hits from a diverse database.

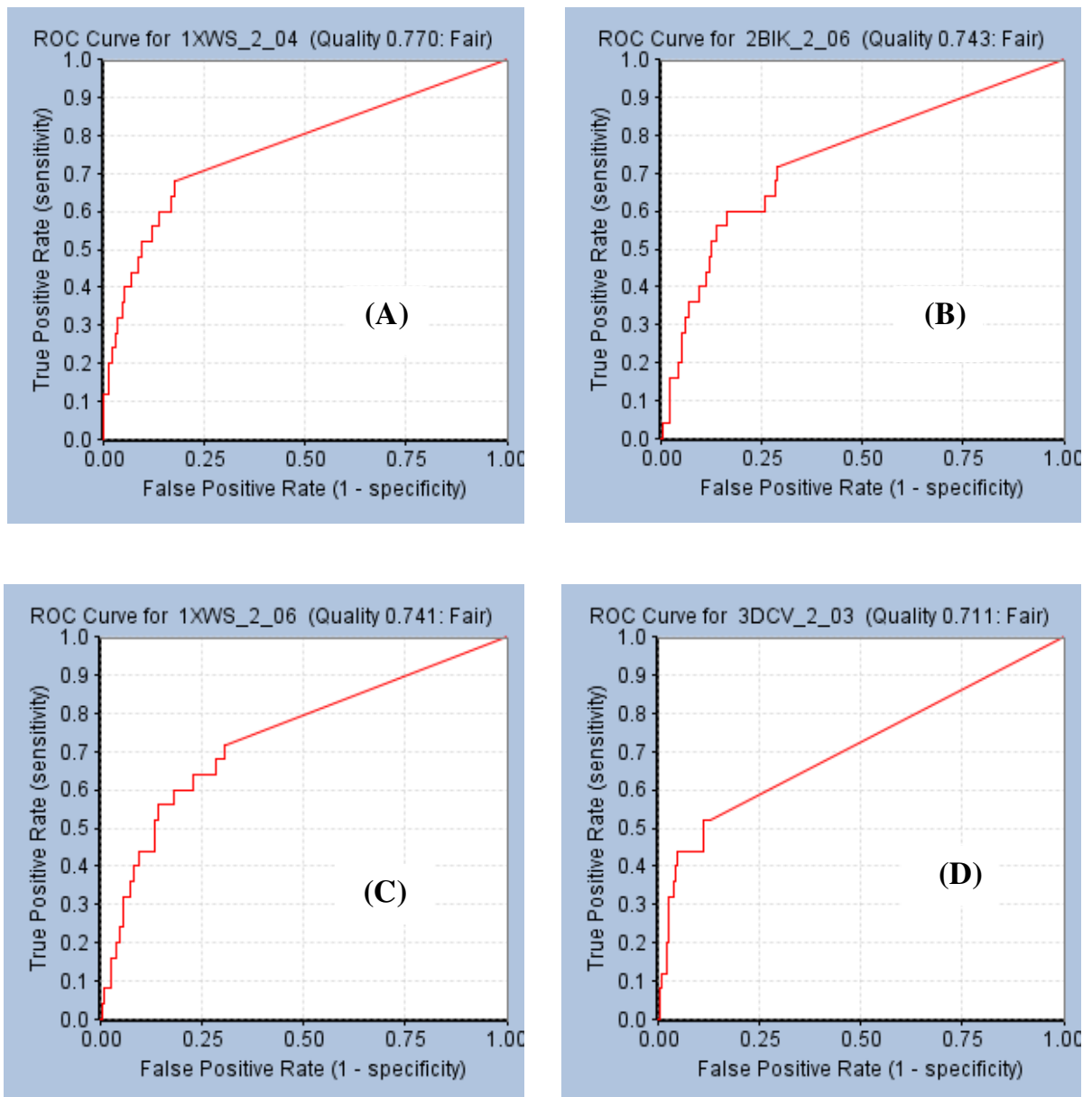


**Figure 1A:** ROC curves of: (A) Hypo1XWS-2-4, (B) Hypo2BIK-2-6, (C) Hypo1XWS-2-6, (D) Hypo3DCV-2-3

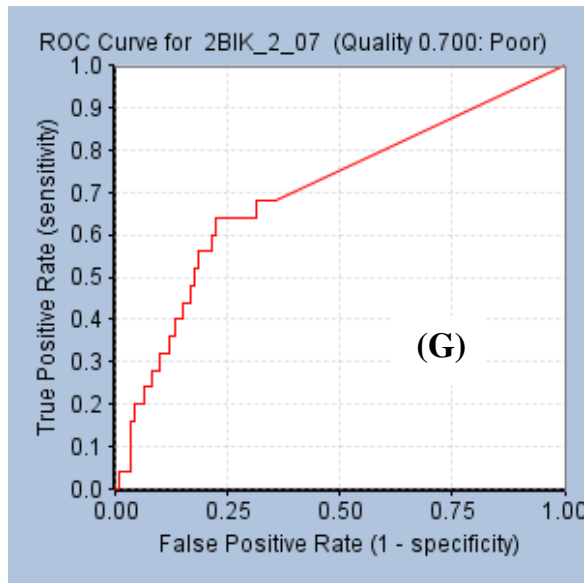
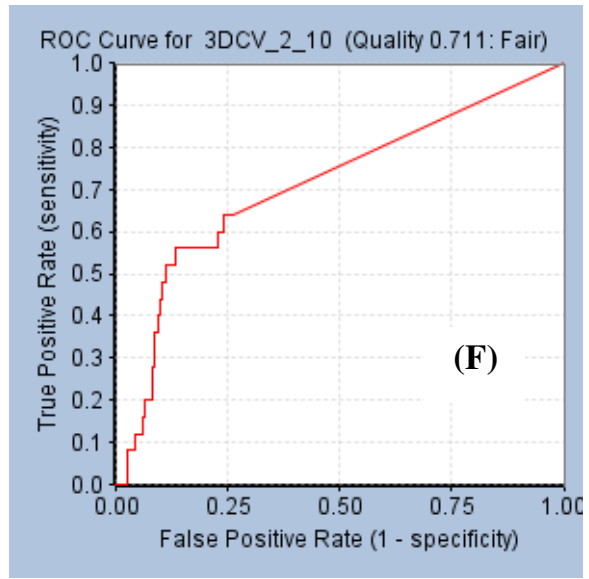
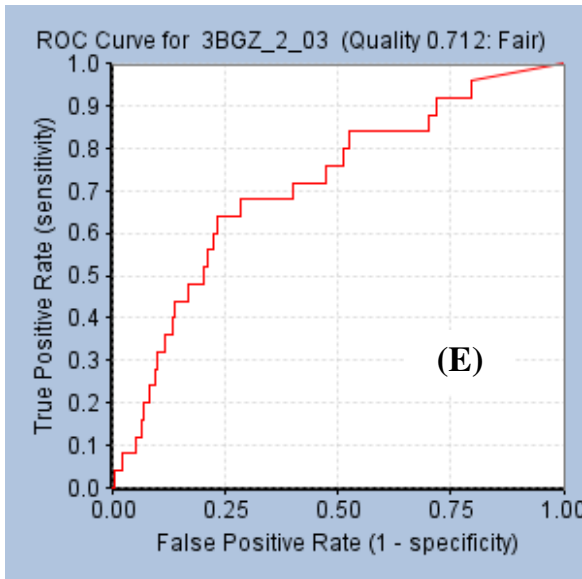


**Figure 1B:** ROC curves of: (E) Hypo3BGZ-2-3, (F) Hypo3DCV-2-10, (G) Hypo2BIK-2-7

**Table 4:** Pharmacophoric features and corresponding weights, tolerances and 3D coordinates of successful pharmacophores.

Model	definition	Chemical Features								
<b>Hypo</b> <b>1XWS-2-4<sup>a</sup></b>		<b>HBD</b>		<b>Hbic</b>		<b>Hbic</b>		<b>Hbic</b>		<b>PosIon</b>
	Weights	1		1		1		1		1
	Tolerances	1.6	2.2	1.6	1.6	1.6	1.6	1.6	1.6	
	Coordinate	X	-20.106	-21.516	-20.54	-20.98	-16.46	-15.866		
		Y	-39.27	-40.621	-36.76	-39.38	-34.26	-36.487		
		Z	-3.549	-5.826	2.7	1.08	-2.8	4.747		
<b>Hypo</b> <b>2BIK-2-6<sup>b</sup></b>		<b>HBA</b>		<b>Hbic</b>		<b>Hbic</b>		<b>Hbic</b>		<b>PosIon</b>
	Weights	1		1		1		1		1
	Tolerances	1.6	2.2	1.6	1.6	1.6	1.6	1.6	1.6	
	Coordinate	X	-41.938	-39.528	-41.94	-44.28	-37.92	-39.325		
		Y	2.759	4.216	0.42	1.4	2.54	4.271		
		Z	4.208	5.244	-2.7	-1.18	2.78	-4.85		
<b>Hypo</b> <b>1XWS-2-6<sup>c</sup></b>		<b>HBA</b>		<b>Hbic</b>		<b>Hbic</b>		<b>Hbic</b>		<b>PosIon</b>
	Weights	1		1		1		1		1
	Tolerances	1.6	2.2	1.6	1.6	1.6	1.6	1.6	1.6	
	Coordinate	X	-18.416	-16.217	-20.54	-20.98	-16.46	-15.866		
		Y	-37.897	-36.802	-36.76	-39.38	-34.26	-36.487		
		Z	-4.292	-6.014	2.7	1.08	-2.8	4.747		
<b>Hypo</b> <b>3DCV-2-3<sup>d</sup></b>		<b>HBD</b>		<b>HBD</b>		<b>RingArom</b>		<b>Hbic</b>		<b>Hbic</b>
	Weights	1		1		1		1		1
	Tolerances	1.6	2.2	1.6	2.2	1.6	1.6	1.6	1.6	1.6
	Coordinate	X	21.576	21.891	17.249	16.118	16.27	15.51	21.56	19.8
		Y	39.548	40	35.147	35.266	35.243	32.33	39.46	37.76
		Z	-1.755	-4.704	-0.14	-2.916	5.387	5.355	1.1	-0.76
<b>Hypo</b> <b>3BGZ-2-3<sup>e</sup></b>		<b>HBA</b>		<b>Hbic</b>		<b>Hbic</b>		<b>Hbic</b>		
	Weights	1		1		1		1		
	Tolerances	1.6	2.2	1.6	1.6	1.6	1.6	1.6	1.6	
	Coordinate	X	-15.997	-14.978	-18.5	-18.96			-21.42	
		Y	35.542	33.858	35.34	38.08		39.82		
		Z	3.31	5.574	-4.58	2.02		-2.7		
<b>Hypo</b> <b>2BIK-2-7<sup>f</sup></b>		<b>HBA</b>		<b>HBD</b>		<b>Hbic</b>		<b>Hbic</b>		<b>Hbic</b>
	Weights	1		1		1		1		1
	Tolerances	1.6	2.2	1.6	2.2	1.6	1.6	1.6	1.6	
	Coordinate	X	-41.938	-39.528	-43.989	-45.858	-41.94	-44.28	-37.92	
		Y	2.759	4.216	1.938	1.381	0.42	1.4	2.54	
		Z	4.208	5.244	3.471	5.751	-2.7	-1.18	2.78	
<b>Hypo</b> <b>3DCV-2-10<sup>g</sup></b>		<b>HBD</b>		<b>HBD</b>		<b>Hbic</b>		<b>Hbic</b>		
	Weights	1		1		1		1		
	Tolerances	1.6	2.2	1.6	2.2	1.6	1.6	1.6	1.6	
	Coordinate	X	21.576	21.891	17.249	16.118	21.56	19.8		
		Y	39.548	40	35.147	35.266	39.46	37.76		
		Z	-1.755	-4.704	-0.14	-2.916	1.1	-0.76		

<sup>a</sup>Hypo **1XWS-2-4** is the 4th hypothesis that resulted from the 1XWS crystal structure.

<sup>b</sup>Hypo **2BIK-2-6** is the 6th hypothesis that resulted from the 2BIK crystal structure.

<sup>c</sup>Hypo **1XWS-2-6** is the 6th hypothesis that resulted from the 1XWS crystal structure.

<sup>d</sup>Hypo **3DCV-2-3** is the 3<sup>rd</sup> hypothesis that resulted from the 3DCV crystal structure.

<sup>e</sup>Hypo **3BGZ-2-3** is the 3<sup>rd</sup> hypothesis that resulted from the 3BGZ crystal structure.

<sup>f</sup>Hypo **2BIK-2-7** is the 7<sup>th</sup> hypothesis that resulted from the 2BIK crystal structure.

<sup>g</sup>Hypo **3DCV-2-10** is the 10<sup>th</sup> hypothesis that resulted from the 3DCV crystal structure.

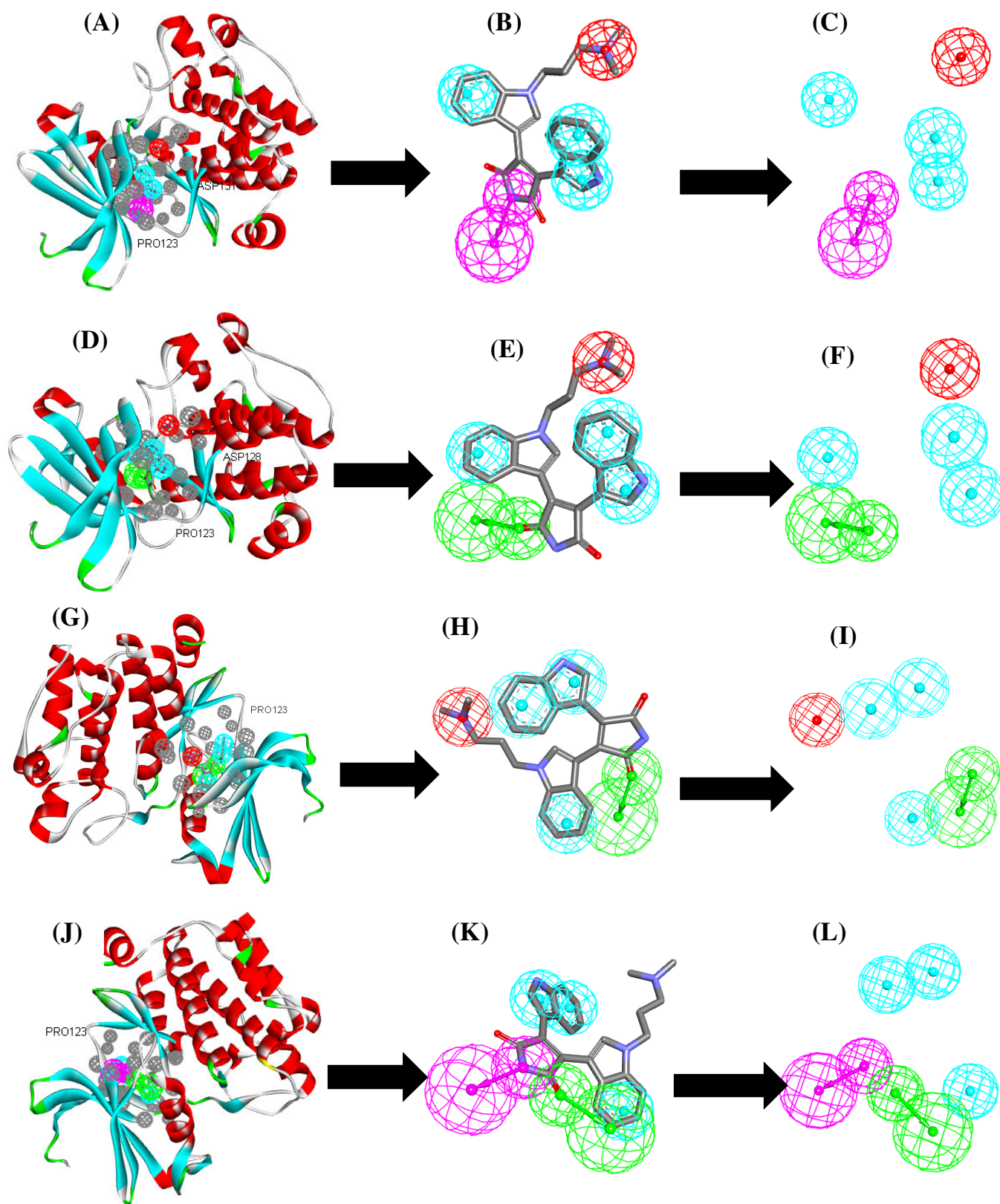


**Figure 2:** (A) Pim-1 kinase crystal (PDB code:1XWS) with the co-crystallized ligand BII1001 and pharmacophore interaction map (B) Co-crystallized ligand BII1001 and pharmacophore 1XWS-2-4, (C)Pharmacophore 1XWS-2-4. (D) Pim-1 kinase crystal (PDB code:1XWS) with the co-crystallized ligand BII1001 and pharmacophore interaction map (E) Co-crystallized ligand BII1001 and pharmacophore 1XWS-2-6, (F)Pharmacophore 1XWS-2-4. (G) Pim-1 kinase crystal (PDB code:2BIK) with the co-crystallized ligand BII1306 and pharmacophore interaction map, (H) Co-crystallized ligand BII1306 and pharmacophore 2BIK-2-6, (I)Pharmacophore 2BIK-2-6. (J) Pim-1 kinase crystal (PDB code:2BIK) with the co-crystallized ligand BII1306 and pharmacophore interaction map, (K) Co-crystallized ligand BII1306 and pharmacophore 2BIK-2-7, (L)Pharmacophore 2BIK-2-7.

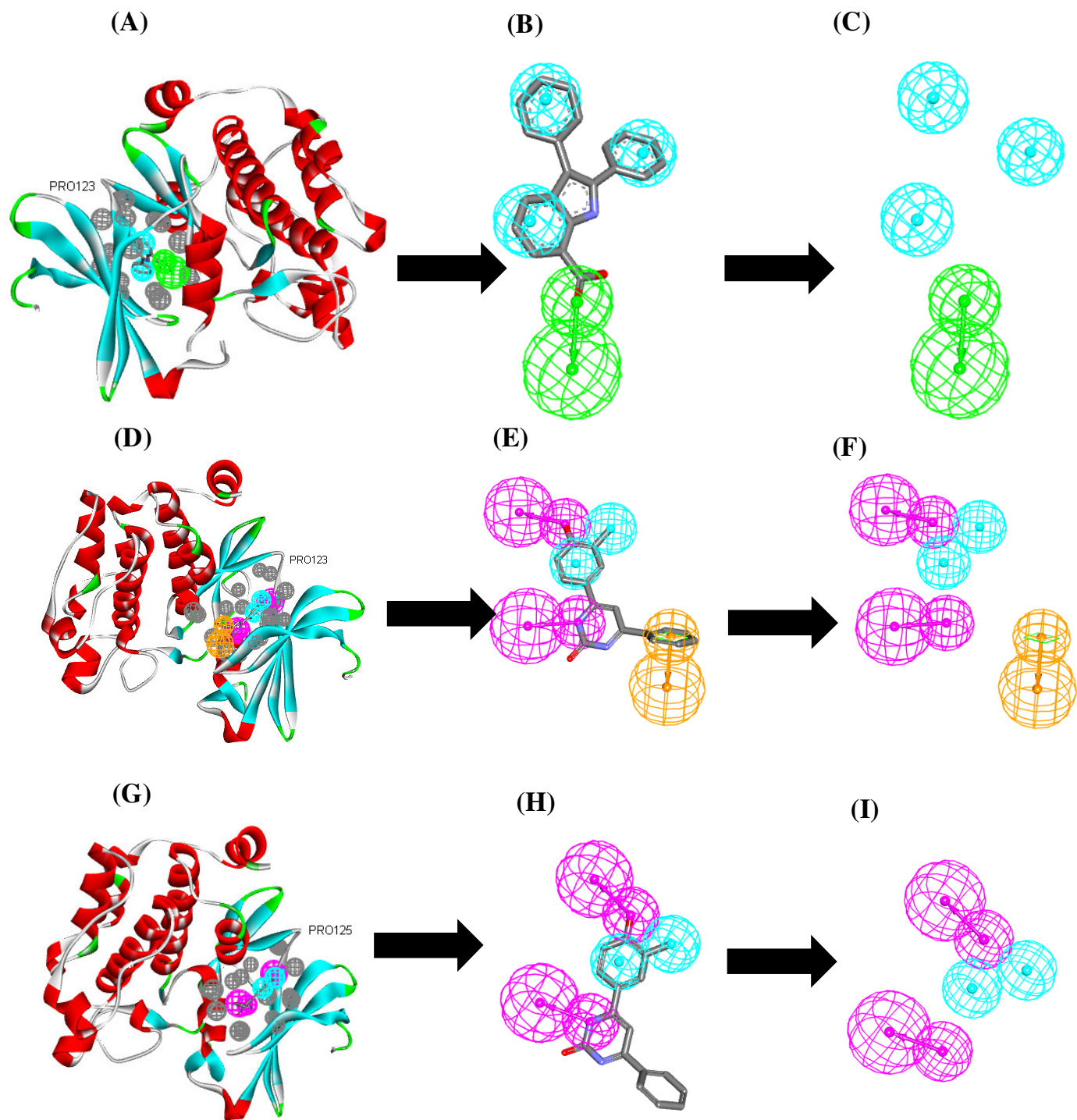


**Figure 3:** (A) Pim-1 kinase crystal (PDB code:3BGZ) with the co-crystallized ligand VX3314 and pharmacophore interaction map (B) Co-crystallized ligand VX3314 and pharmacophore 3BGZ-2-3, (C)Pharmacophore 3BGZ-2-3. (D) Pim-1 kinase crystal (PDB code:3DCV) with the co-crystallized ligand 55E500 and pharmacophore interaction map (E) Co-crystallized ligand 55E500 and pharmacophore 3DCV-2-3, (F)Pharmacophore 3DCV-2-3. (G) Pim-1 kinase crystal (PDB code: 3DCV) with the co-crystallized ligand 55E500 and pharmacophore interaction map, (H) Co-crystallized ligand 55E500 and pharmacophore 3DCV-2-10, (I)Pharmacophore 3DCV-2-10.

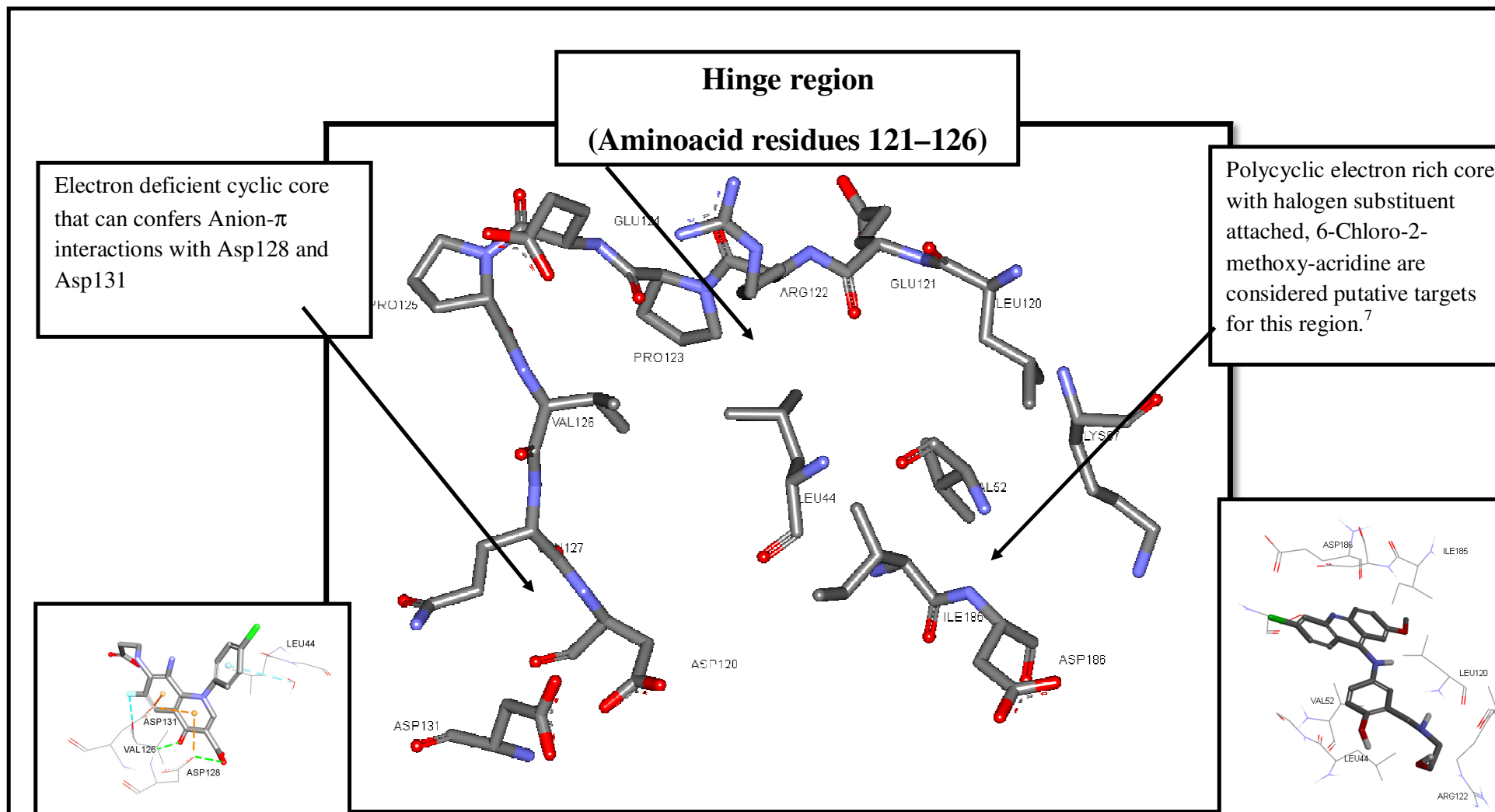


**Figure 4:** Detailed sketch for hinge region Amino acid residues of Pim-1 kinase enzymes, with detailed perspective about the important interaction features inside this binding pocket of Pim-1 kinase.

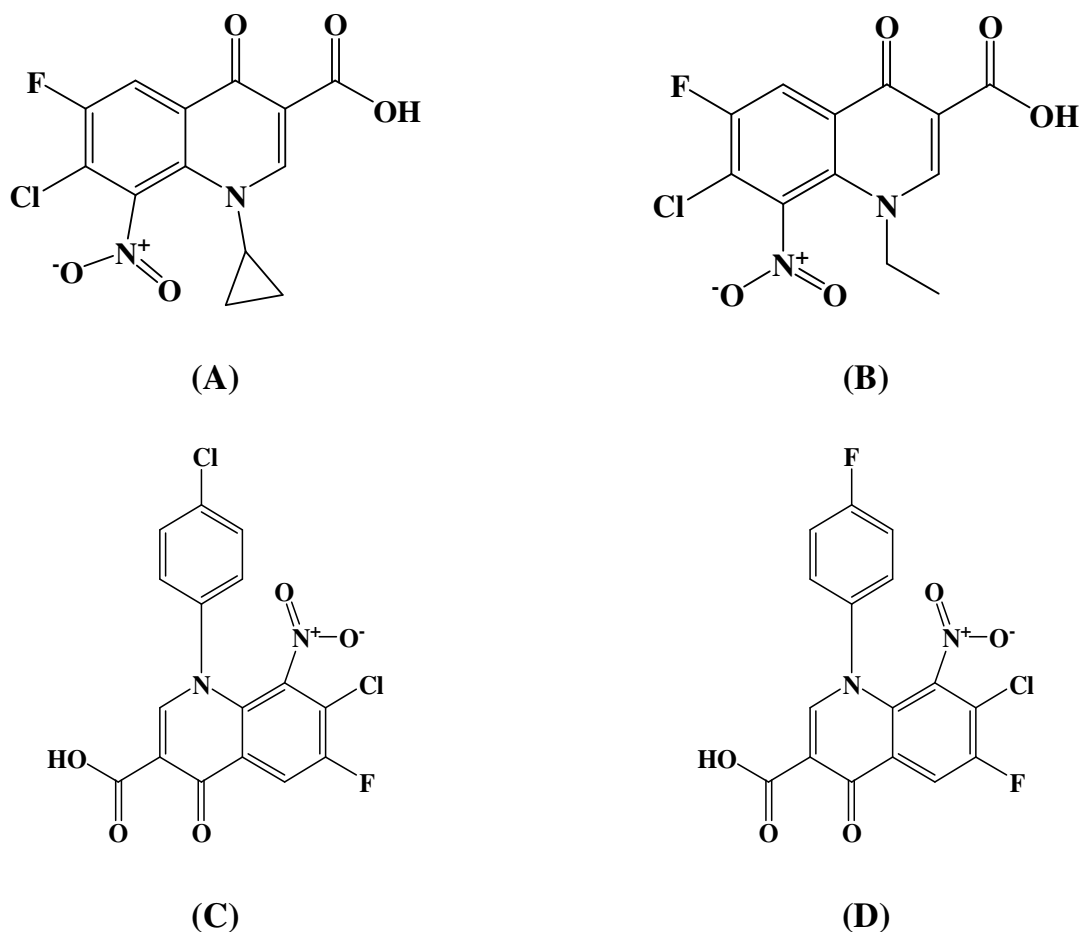


**Figure 5:** Chemical structure of the major synthons used in synthesizing quinolone bases Pim-1 kinase inhibitors (Synthons A, B, C, and D). **(A)** The synthon A: (7-Chloro-1-cyclopropyl -6-fluoro-8-nitro-4-oxo-1,4-dihydroquinoline-3-carboxylic acid). **(B)** The synthon B: (7-Chloro-1-ethyl-6-fluoro-8-nitro-4-oxo-1,4-dihydroquinoline-3-carboxylic acid). **(C)** The synthon C:(7-Chloro-6-fluoro-1-(4-fluoro-phenyl)-8-nitro-4-oxo-1,4-dihydroquinoline-3-carboxylic acid). **(D)** The synthon D:(7-Chloro-1-(4-chloro-phenyl)-6-fluoro-8-nitro-4-oxo-1,4-dihydroquinoline-3-carboxylic acid).

A

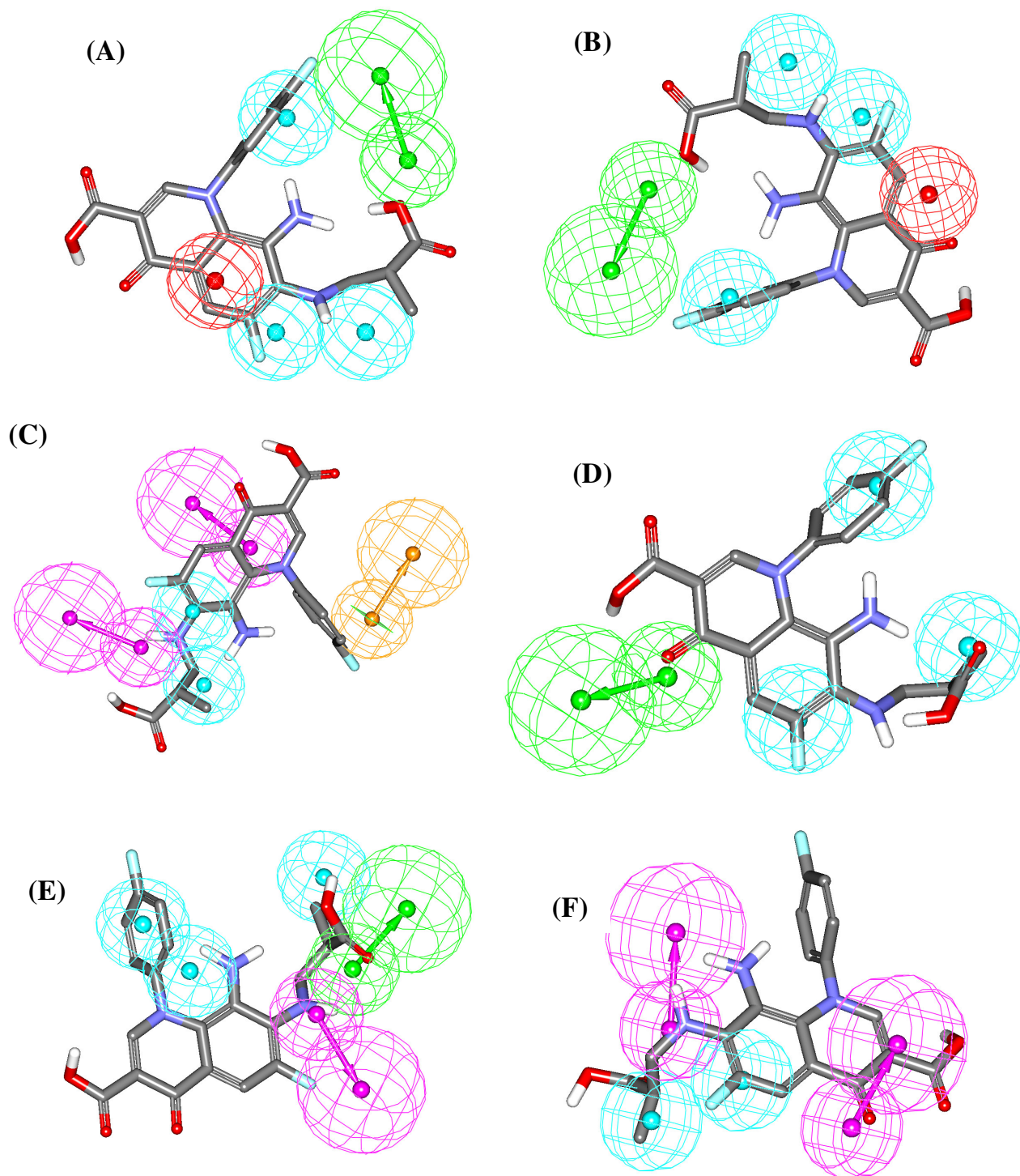


**Figure 6:** Designed compound **39-B** (8-amino-7-((2-carboxypropyl) amino)-6-fluoro-1-(4-fluorophenyl)-4-oxo-1,4-dihydroquinoline-3-carboxylic acid) mapped against: (A) Hypo 2BIK-2-6 (B) Hypo 1XWS-2-6 (C) Hypo 3DCV-2-3 (D) Hypo 3BGZ-2-3 (E) Hypo 2BIK-2-7 (F)Hypo 3DCV-2-10.

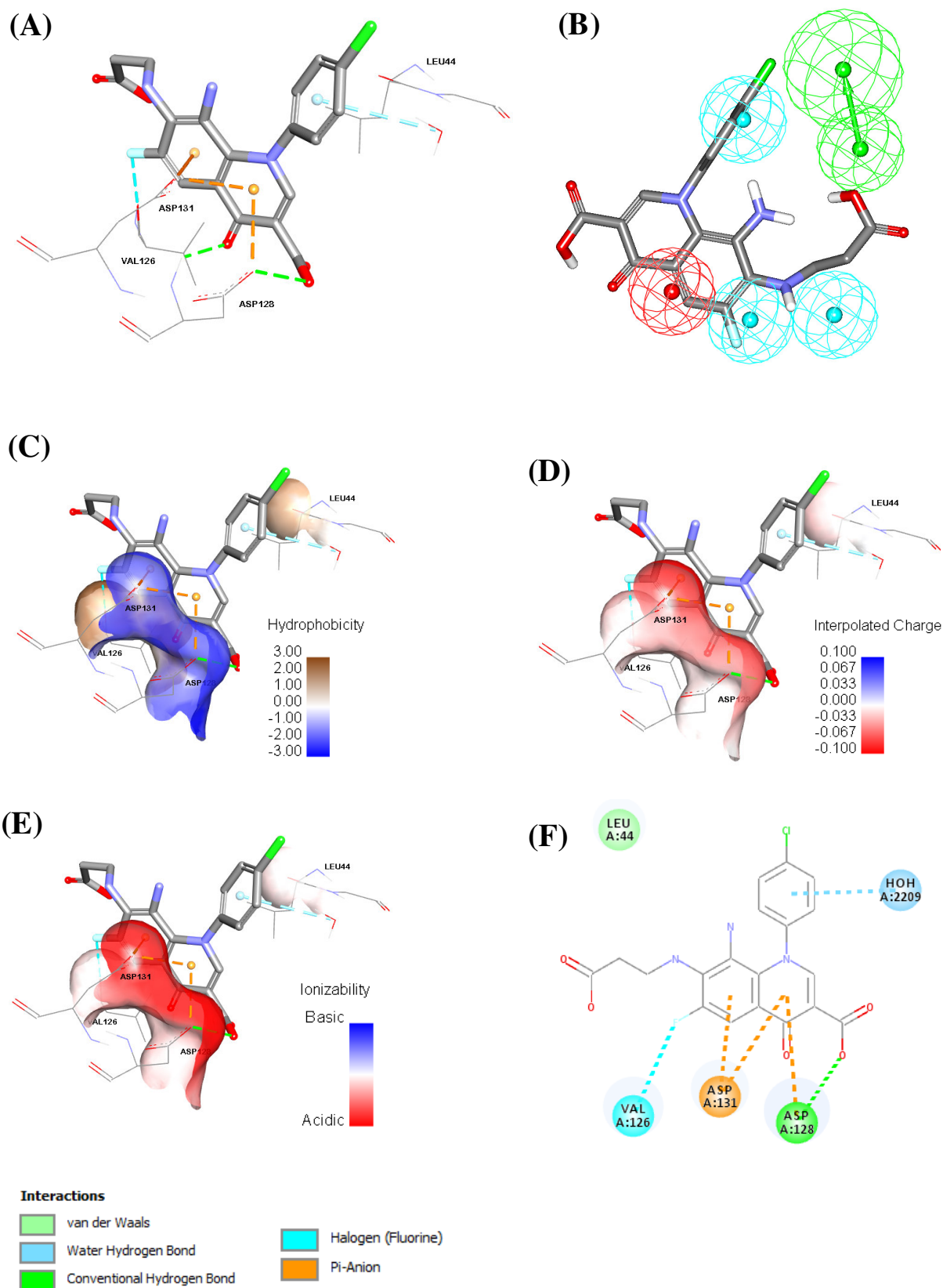


**Figure 7** A. Docked structure of compound **40-B** (IC<sub>50</sub> = 0.2950 μM, Table 5) into Pim-1kinase (PDB code: **1XWS**, 1.8 Å). **B.** Compound **40-B** mapped against pharmacophore **Hypo 1XWS-2-6** **C.** Hydrophobic solvent interaction surface of docked structure of compound **40-B** and Pim-1kinase (PDB code: **1XWS**). **D.** Interpolated charge solvent interaction surface of docked structure of compound **40-B** and Pim-1kinase (PDB code: **1XWS**). **E.** Ionizability solvent interaction surface of docked structure of compound **40-B** and Pim-1kinase (PDB code: **1XWS**). **F.** 2D diagram that shows the main interactions of

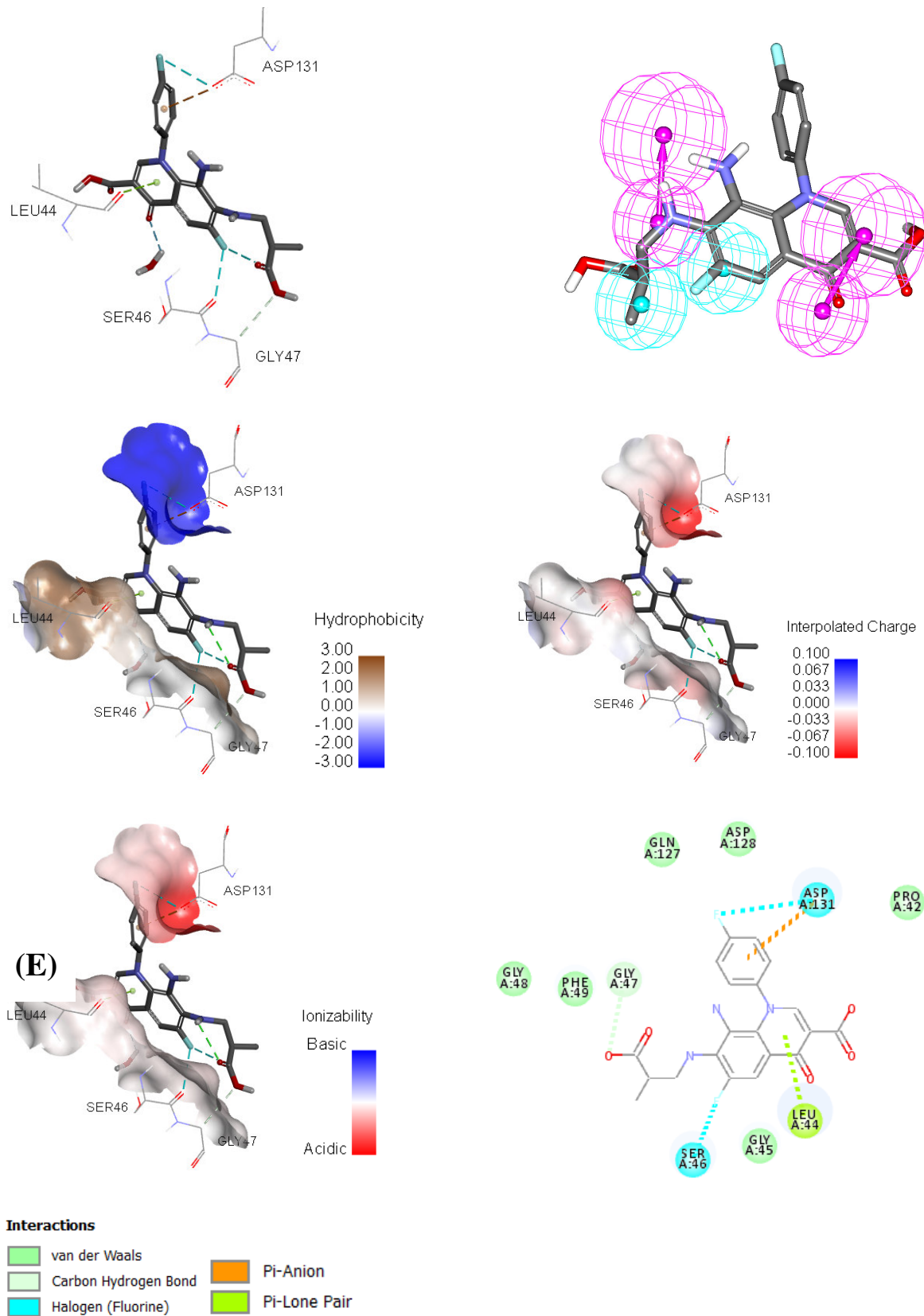
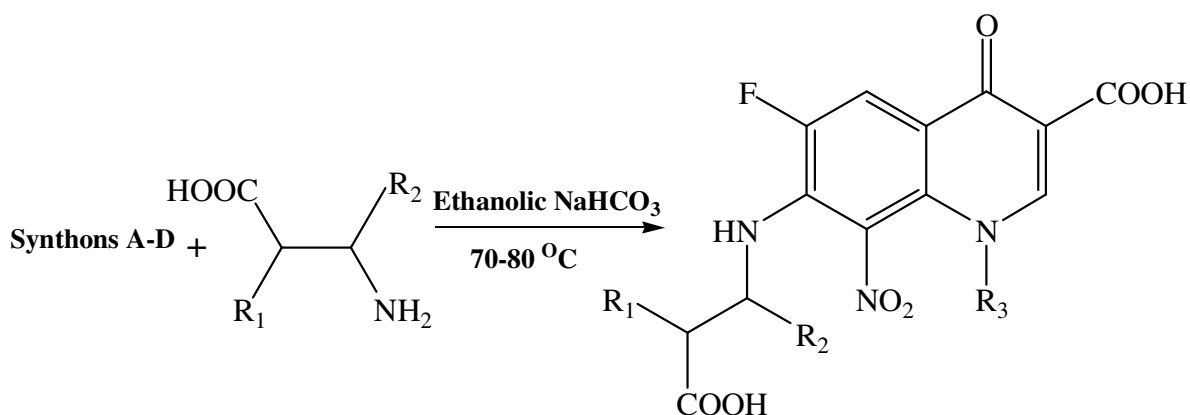


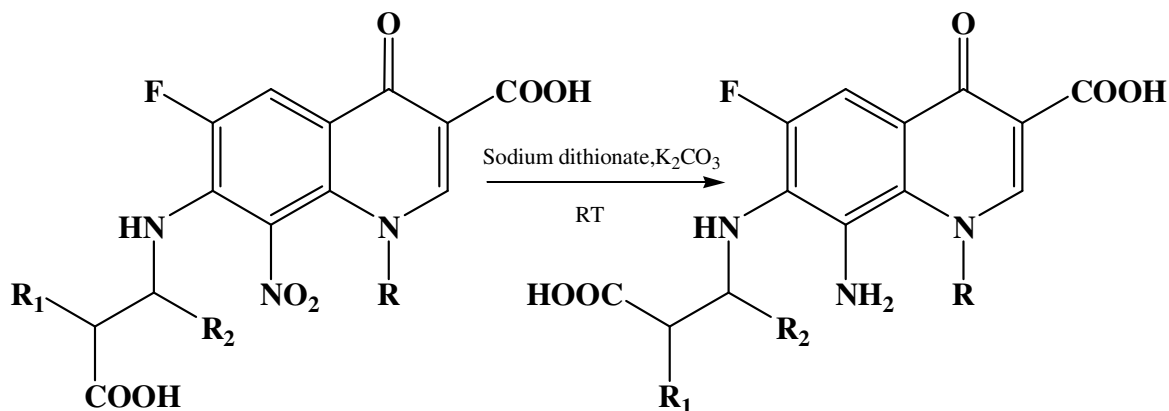
**Figure 8A.** Docked structure of compound **39-B** ( $IC_{50} = 3.335\mu M$ , Table 5) into Pim-1kinase (PDB code: **3DCV**, 2.7 Å). **B.** Compound **39-B** mapped against pharmacophore **Hypo 3DCV-2-10**. Hydrophobic solvent interaction surface of docked structure of compound **39-B** and Pim-1kinase (PDB code: **3DCV**). **C.** Interpolated charge solvent interaction surface of docked structure of compound **39-B** and Pim-1kinase (PDB code: **3DCV**). **D.** Ionizability solvent interaction surface of docked structure of compound **39-B** and Pim-1kinase (PDB code: **3DCV**). **E.** 2D diagram that shows the main interactions of compound **39-A** inside the binding pocket of Pim-1kinase (PDB code: **3DCV**).



**Beta-alanine**  $\text{R}_1 = \text{H}, \text{R}_2 = \text{H}$   
**DL- Aspartic acid**  $\text{R}_1 = \text{H}, \text{R}_2 = \text{COOH}$   
**Isomethyl Beta-alanine**  $\text{R}_1 = \text{CH}_3, \text{R}_2 = \text{H},$

**35**  $\text{R}_1 = \text{H}, \text{R}_2 = \text{H}, \text{R}_3 = \text{Cyclopropyl}$   
**36**  $\text{R}_1 = \text{H}, \text{R}_2 = \text{H}, \text{R}_3 = \text{Ethyl}$   
**37**  $\text{R}_1 = \text{H}, \text{R}_2 = \text{COOH}, \text{R}_3 = \text{Ethyl}$   
**38**  $\text{R}_1 = \text{H}, \text{R}_2 = \text{H}, \text{R}_3 = \text{p-Fluorophenyl}$   
**39-A**  $\text{R}_1 = \text{CH}_3, \text{R}_2 = \text{H}, \text{R}_3 = \text{p-Fluorophenyl}$   
**40-A**  $\text{R}_1 = \text{H}, \text{R}_2 = \text{H}, \text{R}_3 = \text{p-Chlorophenyl}$

**Scheme 1:** Synthesis of (7-Chloro-1-Alkyl-6-fluoro-8-nitro-4-oxo-1,4-dihydroquinoline-3-carboxylic acid) Analogues

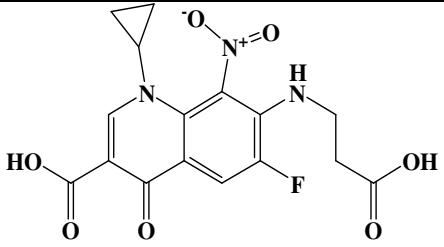
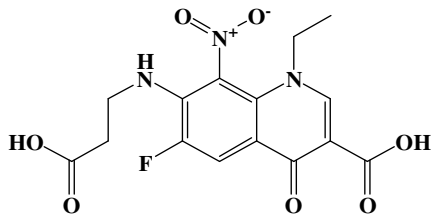
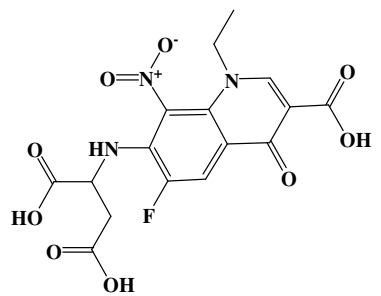


**39-A**  $\text{R}_1 = \text{CH}_3, \text{R}_2 = \text{H}, \text{R}_3 = \text{p-Fluorophenyl}$   
**40-A**  $\text{R}_1 = \text{H}, \text{R}_2 = \text{H}, \text{R}_3 = \text{p-Chlorophenyl}$

**39-B**  $\text{R}_1 = \text{CH}_3, \text{R}_2 = \text{H}, \text{R}_3 = \text{p-Fluorophenyl}$   
**40-B**  $\text{R}_1 = \text{H}, \text{R}_2 = \text{H}, \text{R}_3 = \text{p-Chlorophenyl}$

**Scheme 2:** Synthesis of 8-Amino derivatives of compounds 39-A and 40-A.

**Table 5.** Synthesized hit molecules with their docking scoring function values against Pim-1 kinase (PDB code: 3BGZ) and their in vitro anti-Pim 1 kinase bioactivities.

No. <sup>a</sup>	Structure	Scoring function <sup>b</sup>				Experimental	
		-PLP1	-PLP2	Jain	-PMF	LigandFit docking score	IC <sub>50</sub> (μM) <sup>c</sup>
35		56.01	48.91	-0.9	83.26	32.23	54871
36		44.73	45.74	-0.31	69.36	81.8	56511
37		50.03	40.56	-1.77	77.07	34.68	2.124

<sup>a</sup>See experimental section 4.4 for detailed characterization (NMR, IR, HRMS, Elemental analysis)

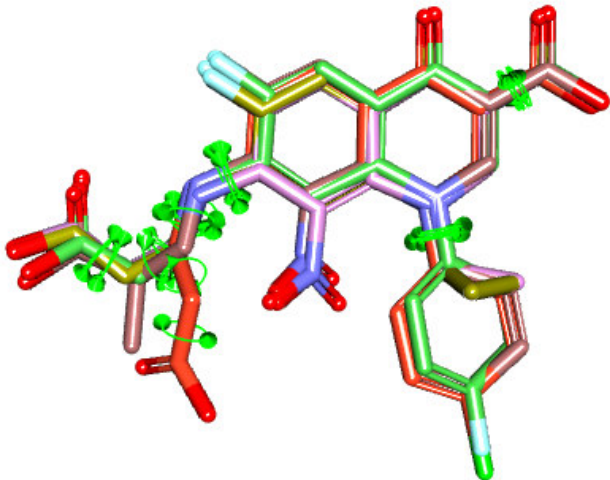
<sup>b</sup>For all optimal docked conformers/poses, scores using the scoring functions were computed, JAIN<sup>32</sup>, PLP1<sup>33,34</sup>, PLP2<sup>33,34</sup>, and PMF<sup>33,34</sup>. The first three are empirical first principle physical interaction terms, while PMF is a knowledge-based potential.

<sup>c</sup>Please refer to figure L under Supplementary Materials for corresponding dose/response curves.

<sup>a</sup>See experimental section 4.4 for detailed characterization (NMR, IR, HRMS, Elemental analysis)

<sup>b</sup>For all optimal docked conformers/poses, scores using the scoring functions were computed, JAIN<sup>32</sup>, PLP1<sup>33,34</sup>, PLP2<sup>33,34</sup>, and PMF<sup>33,34</sup>. The first three are empirical first principle physical interaction terms, while PMF is a knowledge-based potential.

<sup>c</sup>Please refer to figure L under Supplementary Materials for corresponding dose/response curves.

**Table 6:** Alignment of synthesized compounds


Name <sup>a,b</sup>	Overlay similarity / 38	Overlay similarity / 36	Overlay similarity / 35	Overlay similarity / 40-B	Overlay similarity / 39-B
38	1	0.936047	0.943905	0.807548	0.851908
36	0.936047	1	0.9934	0.754918	0.815727
35	0.943905	0.9934	1	0.768972	0.823704
40-B	0.807548	0.754918	0.768972	1	0.883826
39.-B	0.851908	0.815727	0.823704	0.883826	1

<sup>a</sup>Names of compounds as in Table 5

<sup>b</sup>Molecules are aligned using the Manual Alignment protocol implemented in DS 4.5

ACCEPTED MANUSCRIPT

1. Ogawa N, Yuki H Fau - Tanaka A, Tanaka A. Insights from Pim1 structure for anti-cancer drug design. *Expert Opinion on Drug Discovery*. 2012(1746-045X (Electronic)).
2. Schenone S, Tintori C Fau - Botta M, Botta M. Using insights into Pim1 structure to design new anticancer drugs. *Current pharmaceutical design*. 2010(1873-4286 (Electronic)).
3. Blanco-Aparicio C, Carnero A. Pim kinases in cancer: diagnostic, prognostic and treatment opportunities. 2013(1873-2968 (Electronic)).
4. Chen J, Kobayashi M Fau - Darmanin S, Darmanin S Fau - Qiao Y, et al. Hypoxia-mediated up-regulation of Pim-1 contributes to solid tumor formation. 2009(1525-2191 (Electronic)).
5. Pasqualucci L, Neumeister P Fau - Goossens T, Goossens T Fau - Nanjangud G, et al. Hypermutation of multiple proto-oncogenes in B-cell diffuse large-cell lymphomas. 2001(0028-0836 (Print)).
6. Reiser-Erkan C, Erkan M Fau - Pan Z, Pan Z Fau - Bekasi S, et al. Hypoxia-inducible proto-oncogene Pim-1 is a prognostic marker in pancreatic ductal adenocarcinoma. 2008(1555-8576 (Electronic)).
7. Shahin R, Swellmeen L, Shaheen O, Aboalhaja N, Habash M. Identification of novel inhibitors for Pim-1 kinase using pharmacophore modeling based on a novel method for selecting pharmacophore generation subsets. 2016(1573-4951 (Electronic)).
8. Bullock AN, Russo S, Amos A, et al. Crystal Structure of the PIM2 Kinase in Complex with an Organoruthenium Inhibitor. *PLOS ONE*. 2009;4(10): e7112.
9. Backes AC, Zech B, Felber B, Klebl B, Müller G. Small-molecule inhibitors binding to protein kinases. Part I: exceptions from the traditional pharmacophore approach of type I inhibition. *Expert Opinion on Drug Discovery*. 2008;3(12): 1409-1425.
10. Wolber G, Langer T. LigandScout: 3-D pharmacophores derived from protein-bound ligands and their use as virtual screening filters. *Journal of Chemical Information and Modeling*. 2005(1549-9596 (Print)).
11. Wolber G, Langer T. LigandScout: 3-D pharmacophores derived from protein-bound ligands and their use as virtual screening filters. 2005(1549-9596 (Print)).
12. Kirchmair J, Distinto S Fau - Markt P, Markt P Fau - Schuster D, et al. How to optimize shape-based virtual screening: choosing the right query and including chemical information. 2009(1549-9596 (Print)).
13. Kirchmair J, Markt P Fau - Distinto S, Distinto S Fau - Wolber G, Wolber G Fau - Langer T, Langer T. Evaluation of the performance of 3D virtual screening protocols: RMSD comparisons, enrichment assessments, and decoy selection--what can we learn from earlier mistakes? 2008(0920-654X (Print)).
14. Triballeau N, Acher F, Brabet I, Pin J-P, Bertrand H-O. Virtual Screening Workflow Development Guided by the "Receiver Operating Characteristic" Curve Approach. Application to High-Throughput Docking on Metabotropic Glutamate Receptor Subtype 4. *Journal of Medicinal Chemistry*. 2005;48(7): 2534-2547.
15. Halligan S, Altman Dg Fau - Mallett S, Mallett S. Disadvantages of using the area under the receiver operating characteristic curve to assess imaging tests: a discussion and proposal for an alternative approach. *European radiology*. 2015(1432-1084 (Electronic)).
16. Discovery Studio 4.5 User Guide Biovia (Accelrys) Software Inc. San Diego; 2016.
17. Alkorta I, Rozas I, Elguero J. Interaction of Anions with Perfluoro Aromatic Compounds. *Journal of the American Chemical Society*. 2002;124(29): 8593-8598.
18. de Hoog P, Gamez P, Mutikainen I, Turpeinen U, Reedijk J. An Aromatic Anion Receptor: Anion- $\pi$  Interactions do Exist. *Angewandte Chemie*. 2004;116(43): 5939-5941.
19. Wang D-X, Wang M-X. Anion- $\pi$  Interactions: Generality, Binding Strength, and Structure. *Journal of the American Chemical Society*. 2013;135(2): 892-897.
20. Murray-Rust P, Stallings WC, Monti CT, Preston RK, Glusker JP. Intermolecular interactions of the carbon-fluorine bond: the crystallographic environment of fluorinated

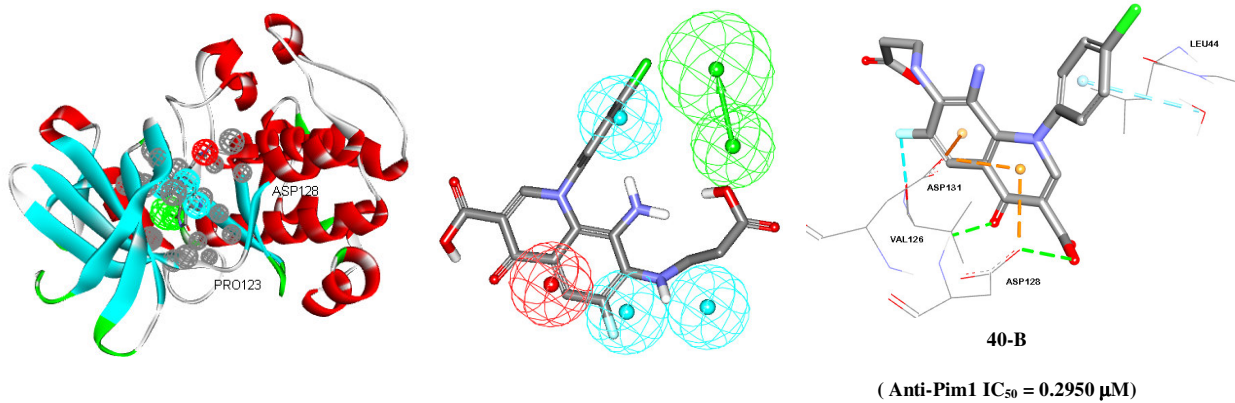
- carboxylic acids and related structures. *Journal of the American Chemical Society*. 1983;105(10): 3206-3214.
21. Shahin R, Alqtaishat S Fau - Taha MO, Taha MO. Elaborate ligand-based modeling reveal new submicromolar Rho kinase inhibitors. 2011(1573-4951 (Electronic)).
  22. Akué-Gédu R, Rossignol E, Azzaro S, et al. Synthesis, Kinase Inhibitory Potencies, and in Vitro Antiproliferative Evaluation of New Pim Kinase Inhibitors. *Journal of Medicinal Chemistry*. 2009;52(20): 6369-6381.
  23. Cheney IW, Yan S, Appleby T, et al. Identification and structure–activity relationships of substituted pyridones as inhibitors of Pim-1 kinase. *Bioorganic & Medicinal Chemistry Letters*. 2007;17(6): 1679-1683.
  24. Nishiguchi GA, Atallah G Fau - Bellamacina C, Bellamacina C Fau - Burger MT, et al. Discovery of novel 3,5-disubstituted indole derivatives as potent inhibitors of Pim-1, Pim-2, and Pim-3 protein kinases. *Bioorganic & Medicinal Chemistry Letters*. 2011(1464-3405 (Electronic)).
  25. Pastor J, Oyarzabal J, Saluste G, et al. Hit to lead evaluation of 1,2,3-triazolo[4,5-b]pyridines as PIM kinase inhibitors. *Bioorganic & Medicinal Chemistry Letters*. 2012;22(4): 1591-1597.
  26. Pierre F, Stefan E Fau - Nedellec A-S, Nedellec As Fau - Chevrel M-C, et al. 7-(4H-1,2,4-Triazol-3-yl)benzo[c][2,6]naphthyridines: a novel class of Pim kinase inhibitors with potent cell antiproliferative activity. 2011(1464-3405 (Electronic)).
  27. Taha MO, Qandil Am Fau - Zaki DD, Zaki Dd Fau - AlDamen MA, AlDamen MA. Ligand-based assessment of factor Xa binding site flexibility via elaborate pharmacophore exploration and genetic algorithm-based QSAR modeling. 2005(0223-5234 (Print)).
  28. Venkatachalam CM, Jiang X Fau - Oldfield T, Oldfield T Fau - Waldman M, Waldman M. LigandFit: a novel method for the shape-directed rapid docking of ligands to protein active sites. *Journal of Molecular Graphics and Modelling* 2003(1093-3263 (Print)).
  29. Al-Hiari MY, Abu-Dahab R, El-Abadelah MM. Heterocycles [h]-Fused Onto 4-Oxoquinoline-3-Carboxylic Acid, Part VIII [1]. Convenient Synthesis and Antimicrobial Properties of Substituted Hexahydro[1,4]diazepino[2,3-h]quinoline-9-carboxylic acid and Its Tetrahydroquino[7,8-b]benzodiazepine Analog. *Molecules*. 2008;13(11).
  30. Al-Hiari YM, Kasabri V, Shakya AK., Alzweiri MH, Afifi FU, Bustanji YK, Al-Masri IM. Fluoroquinolones: Novel class of gastrointestinal lipid digestion and absorption inhibitors. *Medicinal Chemistry Research* 2014 DOI :10.1007/s00044-014-0913-4
  31. Al-Hiari YM, Shakya AK, Al-rajab WJ, Abdel Rahim EA, Alzweiri MH, Rustam L, Darwish R. Antimicrobial screening of novel N-4- fluorophenylquino-[7,8-b][1,4]- benzodiazepin-3-carboxylic acid derivatives. *Revue Roumaine De Chimie*. 2015; 60(9): 899–905.
  32. Jain AN. Scoring non-covalent protein–ligand interactions: a continuous differentiable function tuned to compute binding affinities, *Journal of Computer Aided Molecular Design*. 1996; 10: 427–440.
  33. Krammer A, Kirchoff PD, Jiang X, Venkatachalam CM, Waldman M. LigScore: a novel scoring function for predicting binding affinities, *Journal of molecular graphics and modelling*. 2005; 23: 395–407.
  34. Muegge I. A knowledge-based scoring function for protein–ligand interactions: probing the reference state, *Perspect. Drug Discovery*. 2000; 20: 99–114.

## Research Highlights

- 104 crystal structure of Pim-1 kinase were collected from the Protein Data Bank.
- The co-crystallized ligand-Pim 1 kinase receptor interactions were modelled.
- 111 pharmacophores were generated of which 7 were superior in their ROC GFA validation performance
- Optimal Hypogen models were used as 3D queries to synthesize Quinone based Pim-1 kinase inhibitors
- The most potent hits exhibited  $IC_{50}$  values of 0.29  $\mu$ M against Pim-1 kinase.

ACCEPTED MANUSCRIPT

## Graphical Abstract



ACCEPTED MANUSCRIPT